Mixing by Oceanic Lee Waves. AUTHOR'S VERSION, NOT INCLUDING ARFM COPY-EDITS, OR ARFM-MODIFICATIONS TO FIGURES. AUTHOR'S CORRECTIONS IN RESPONSE TO REVIEW ARE INCLUDED.

Sonya Legg,[1] [1]Atmospheric and Oceanic Sciences, Princeton University, Princeton, USA, NJ 08540; email: slegg@princeton.edu

June 10, 2021

Abstract

Oceanic lee-waves are generated in the deep stratified ocean by the flow of ocean currents over sea-floor topography, and when they break, can lead to mixing in the stably-stratified ocean interior. While the theory of linear lee-waves is well established, the nonlinear mechanisms leading to mixing are still under investigation. Tidally-driven lee-waves have long been observed in the ocean, along with associated mixing, but observations of lee-waves forced by geostrophic eddies are relatively sparse and largely indirect. Parameterizations of the mixing due to ocean lee-waves are now being developed and implemented in ocean climate models. This review summarizes current theory and observations of lee-wave generation, and mixing driven by lee-wave breaking, distinguishing between steady and tidally-oscillating forcing. The existing parameterizations of lee-wave-driven mixing informed by theory and observations are outlined, and the impacts of the parameterized lee-wave-driven mixing on simulations of large-scale ocean circulation are summarized.

oceanic lee-waves, internal waves, stratified turbulence, mixing parameterization

Contents

1 INTRODUCTION

Lee-waves are waves in a fluid which is stably stratified in buoyancy, forced by flow over an obstacle (e.g. a mountain range in the atmosphere, sea-floor topography in the ocean) (Bell Jr., 1975, Long, 1955, Scorer, 1949) (**Figure 1**). The waves generated by a steady flow are stationary from the perspective of a stationary observer, but associated with a finite Doppler shifted frequency in the frame of reference moving with the flow. In the atmosphere, lee-waves are most easily observed in the form of lenticular clouds over their crests in the lee (i.e. downstream) of the topography (Conover, 1964); hence the name lee-waves. Lee-waves have a long history of study in the atmosphere (Wurtele et al., 1996), leading to local effects such as downslope windstorms (Peltier & Clark, 1979) and distributed effects such as impacts on large-scale flow (McFarlane, 1987). Locally, the mean flow exerts a drag on the topography, transferring momentum and energy to the vertically propagating waves which deposit that momentum and energy when they break higher in the atmosphere (Broad, 1995, Teixeira, 2014). Parameterizations of orographic gravity-wave drag are a key component of large-scale atmospheric models (Palmer et al., 1986).

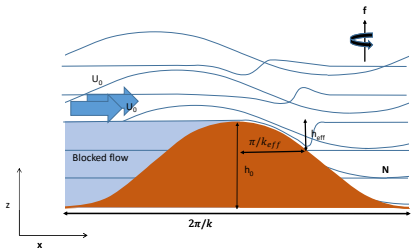

Figure 1: Schematic of lee-wave generation, showing key parameters, for (top) linear regime where $Nh_0/U_0 < 1$ and $f < U_0 k < N$; (bottom) nonlinear regime, where $Nh_0/U_0 > 1$. Isopycnals are indicated in blue.

In the ocean, lee-wave generation also leads to drag on the larger-scale flow (Trossman et al., 2016), but the role of lee-waves in driving mixing in the otherwise largely adiabatic ocean interior is potentially more important than in the atmosphere (MacKinnon et al., 2017). Lee-waves provide a mechanism for extracting energy from the geostrophic flow, and transferring that energy to small-scale turbulence when the waves break. The turbulence in turn leads to a dissipative loss of mechanical energy, as well as an irreversible transfer from kinetic energy to potential energy, as parcels of fluid of different density are stirred and mixed together (Winters et al., 1995). Hence, lee-waves can play an important role in both the global energy budget (Trossman et al., 2013, Nikurashin & Ferrari, 2011) and in mixing of tracers across density surfaces in the stably stratified ocean interior (Melet et al., 2014).

Whereas in the atmosphere, lee waves are often generated by large-scale jets flowing over mountain ranges (Alexander & Teitelbaum, 2011), in the ocean significant bottom velocities, necessary to generate finite-amplitude lee-waves, are often associated with mesoscale eddies (Ferrari & Wunsch, 2009), with spatial scales of order 5-100km, and timescales varying from weeks to months. Tidal flow can also generate transient lee-waves (Alford et al., 2014).

Recent research into ocean lee-waves has focused on both those generated by geostrophic flow, and tidal flow, with a over-riding goal of developing parameterizations of the drag on the large-scale flow and the mixing induced by the breaking lee-waves (MacKinnon et al., 2017). While the drag and mixing are connected, here I will largely focus on the mixing, its prediction, observation, and parameterization, as well as the impacts of mixing on large-scale circulation. The focus is primarily on lee-waves driven by geostrophic flow; however, tidally-driven lee-waves will also be discussed since direct observations of breaking lee-waves are easier to obtain in the more predictable tidally-driven regime.

I will begin with an outline of the linear theory for the generation of lee-waves by both steady and oscillating flows, followed by the important nonlinear regimes, and mechanisms which cause lee-waves to break, leading to mixing. These theoretical, numerical and laboratory predictions will be compared with observations of lee-waves and lee-wave driven mixing in the ocean. I will explore some of the discrepancies between observations and predictions, and attempt to reconcile the two. I will then summarize the current efforts to parameterize mixing by ocean lee-waves, and the impact of these parameterizations on simulations of the large-scale ocean circulation and climate. Finally, I will outline the knowledge gaps which still remain.

2 THEORY AND LABORATORY AND NUMERICAL SIMULATION OF OCEANIC LEE WAVES

2.1 Linear theory for lee wave generation: steady flow

Lee-waves are quasi-steady waves generated by stratified flow over topography. Following Bell Jr. (1975) we will therefore begin by deriving the linear solutions for flow over topography, using the incompressible inviscid Boussinesq fluid equations in the presence of planetary rotation:

$$\frac{D\mathbf{u}}{Dt} + 2\mathbf{\Omega} \times \mathbf{u} = \frac{-\nabla p}{\rho_0} + b\hat{\mathbf{z}} \tag{1}$$

$$\nabla.\mathbf{u} = 0 \tag{2}$$

$$\frac{Db}{Dt} = 0 \tag{3}$$

where $\mathbf{u} = u\hat{\mathbf{x}} + v\hat{\mathbf{y}} + w\hat{\mathbf{z}}$ is the velocity vector, and $\hat{\mathbf{x}}$, $\hat{\mathbf{y}}$, and $\hat{\mathbf{z}}$ are the unit vectors in the x, y and z directions respectively. The z direction is aligned with the gravitational vector. $\frac{D}{Dt}$ is the material derivative:

$$\frac{D}{Dt} = \frac{\partial}{\partial t} + \mathbf{u}.\nabla \tag{4}$$

$\mathbf{\Omega}$ is the planetary rotation vector, p is the pressure, ρ_0 is a reference density, and b is the buoyancy:

$$b = -g\rho/\rho_0 \tag{5}$$

where g is the gravitational acceleration and ρ is the fluid density, and ρ_0 is a reference density. By assuming b is a conserved quantity, we are ignoring any fluxes of buoyancy in or out of the fluid, as well as assuming a linear equation of state, relating density to the conserved quantities, temperature and salinity. We make the f-plane approximation: $2\mathbf{\Omega} = f\hat{\mathbf{z}}$, where f is a constant Coriolis parameter. Now we specify a basic state with buoyancy dependent on vertical coordinate only, $b = b_0(z)$ and flow $\mathbf{u} = U_0\hat{\mathbf{x}}$, where U_0 is a constant. For convenience we orientate our axes so that $U_0 > 0$ throughout. This steady basic state satisfies:

$$\frac{\partial p_0}{\partial z} = \rho_0 b_0(z) \tag{6}$$

and

$$f\rho_0 U_0 = -\frac{\partial p_0}{\partial y} \tag{7}$$

Defining the buoyancy frequency N:

$$N^2 = \frac{db_0}{dz} \tag{8}$$

where we will assume that N is a function only of z, we linearize about this basic state, identifying the perturbation quantities by the superscript $'$:

$$\left[\frac{\partial}{\partial t} + U_0\frac{\partial}{\partial x}\right]u' - fv' = -\frac{1}{\rho_0}\frac{\partial p'}{\partial x} \;;\; \left[\frac{\partial}{\partial t} + U_0\frac{\partial}{\partial x}\right]v' + fu' = -\frac{1}{\rho_0}\frac{\partial p'}{\partial y} \;;\; \left[\frac{\partial}{\partial t} + U_0\frac{\partial}{\partial x}\right]w' = -\frac{1}{\rho_0}\frac{\partial p'}{\partial z} + b' \tag{9}$$

$$\left[\frac{\partial}{\partial t} + U_0\frac{\partial}{\partial x}\right]b' + w'N^2 = 0 \tag{10}$$

along with the incompressibility equation. Looking for steady solutions, we obtain the wave equation:

$$U_0^2\frac{\partial^2}{\partial x^2}\nabla^2 w' + f^2\frac{\partial^2 w}{\partial z^2} + N^2\nabla_H^2 w' = 0 \tag{11}$$

We will find solutions to this equation in a semi-infinite domain, subject to no normal flow at the bottom boundary ($w = \mathbf{u}.\nabla h$), with upward wave energy flux. For simplicity, we will first examine waves generated by flow over monochromatic sinusoidal topography (**Figure 1a**) of the form:

$$h = h_0 sin(kx), \tag{12}$$

where for convenience, we assume $k > 0$. The linearized bottom boundary condition becomes:

$$w = U_0 \frac{\partial h}{\partial x} = h_0 U_0 k cos(kx) \tag{13}$$

We assume the amplitude of the topography is small (the weak topography assumption), so this boundary condition is applied at $z = 0$.

Now assuming constant N, we choose a solution to satisfy the lower boundary condition of the form

$$w = h_0 U_0 k cos(kx + mz) \tag{14}$$

which on substitution into eqn 11 gives the dispersion relation:

$$m^2 = k^2 \frac{(N^2 - \omega_d^2)}{(\omega_d^2 - f^2)} \tag{15}$$

where ω_d is the Doppler shifted or intrinsic frequency, $\omega_d = \omega_s - U_0 k$, and ω_s is the frequency in the resting frame. When $\omega_s = 0$, then $\omega_d = -U_0 k$. The vertical wave number m is real (i.e. a vertically propagating wave solution) only if

$$f < U_0 k < N \tag{16}$$

Outside these limits, the perturbation will be evanescent, and decay away from the topography. In the ocean, with relatively small bottom velocities compared to the atmosphere, this restricts lee-wave generation to topography with small horizontal length-scales: $\lambda \leq U_0/f \sim O(1km)$ for typical bottom flow speeds in a high latitude ocean.

In the limit of $f << U_0 k << N$

$$m \approx \frac{N}{U_0} \tag{17}$$

and the vertical length-scale is (Klymak et al., 2010a)

$$\lambda_0 = 2\pi/m = 2\pi U_0/N \tag{18}$$

The positive root for m (eqn 15) gives an upward energy flux, equal to the rate of energy conversion per unit area,

$$C = < p'w' > = \frac{1}{2} \rho_0 \frac{k}{m} h_0^2 U_0 (N^2 - U_0^2 k^2) \tag{19}$$

as required for energy propagation away from the topography. Substituting for m we have

$$C = \frac{1}{2} \rho_0 U_0 h_0^2 \sqrt{(U_0^2 k^2 - f^2)} \sqrt{(N^2 - U_0^2 k^2)} \tag{20}$$

In the linear limit, outside of the range $f < U_0 k < N$ the perturbations will lead to zero net energy flux.

Generalizing to topography characterized by a 2D height spectrum $P(\mathbf{k})$, where $\mathbf{k} = (k, l)$ is the topographic wavenumber, we obtain (Bell Jr., 1975, Nikurashin & Ferrari, 2010a):

$$C = \frac{\rho_0}{4\pi^2} \int_{-\infty}^{+\infty} \int_{-\infty}^{+\infty} \frac{\mathbf{U_0}.\mathbf{k}}{|\mathbf{k}|} P(\mathbf{k}) \sqrt{((\mathbf{U_0}.\mathbf{k})^2 - f^2)} \sqrt{(N^2 - (\mathbf{U_0}.\mathbf{k})^2)} d\mathbf{k} \tag{21}$$

The linear wave solutions considered thus far propagate energy upward with a depth independent energy flux. Energy can only be used for mixing if there is divergence of the vertical energy flux, i.e. if the waves break. Understanding how lee-waves can lead to mixing therefore requires us to understand nonlinear waves.

For linear theory to apply, the perturbation velocities must be small relative to the background flow, i.e. $|u'/U_0| << 1$. For $N >> U_0 k >> f$,

$$|\frac{u'}{U_0}| \approx \frac{N h_0}{U_0} \tag{22}$$

and so linear theory applies only if

$$Fr_L = \frac{N h_0}{U_0} << 1 \tag{23}$$

This parameter Fr_L has referred to as the inverse Froude number (Drazin, 1961) and the Long number (Aguilar & Sutherland, 2006). Since Mayer & Fringer (2017) showed that Fr_L is the ratio between the lee wave vertical fluid velocity and vertical group velocity, w'/C_{gz}, i.e. the vertical wave Froude number, and the magnitude of this parameter determines the nonlinearity of the lee-waves, we therefore refer to this parameter as the "lee wave Froude number" . This single parameter controls much of the behavior of the lee-wave problem, along with frequency ratios $N/(U_0k)$ and $f/(U_0k)$. Fr_L is also a measure of the steepness of the topography relative to the steepness of the wave characteristic (Nikurashin & Ferrari, 2010b):

$$\frac{\text{topographic steepness}}{\text{wave characteristic steepness}} = \frac{h_0 k}{k/m} = \frac{h_0 k}{\sqrt{\frac{U_0^2 k^2 - f^2}{N^2 - U_0^2 k^2}}} \approx \frac{N h_0}{U_0} \tag{24}$$

where the approximation applies if $N >> U_0 k >> f$. Fr_L is also proportional to the square root of the ratio between the potential energy change due to lifting a parcel of fluid the height of the topography and the kinetic energy available in the mean flow. When $Fr_L > 1$ the mean flow is energetically unable to move fluid parcels over the height of the topography, and blocking will occur on the upstream side of the topography (SMITH, 1989). The effective height of the topography over which the flow moves is then reduced so as to maintain a Froude number of 1, i.e. $Nh_{eff}/U_0 \sim 1$ so that $h_{eff} \sim U_0/N$ is the distance by which fluid is displaced below the topographic peak (Winters & Armi, 2012) (**Figure 1b**). The horizontal topographic lengthscale experienced by the flow is similarly reduced to h_{eff}/α_t where α_t is the topographic aspect ratio (height/width) at the top of the topography, and the intrinsic frequency of the wave then becomes $U_0 k_{eff} \sim N\alpha_t$, with $U_0 k_{eff} < N$ required for propagating waves (E. Mayer and O. Fringer, unpublished manuscript).

2.2 Linear theory for lee wave generation: oscillating flow

Transient lee-waves can also be generated by time-dependent flow, with the oscillating flow of the barotropic tides being particularly relevant in the context of ocean mixing. The oscillating tidal flow also excites internal waves at the tidal forcing frequency (internal tides) (Bell, 1975), and our goal here is not to reproduce the vast literature on internal tide generation (see Garrett & Kunze (2007)). Instead, we will focus on when and how tidal flow can generate lee-waves (i.e. stationary waves with an intrinsic frequency $\omega = -U_0 k$), in addition to or in place of propagating internal waves at the tidal frequency.

For a background flow given by $U = U_0 cos(\omega_0 t)$ over a topography of the form $h = h_0 sin(kx)$, the form of the linear perturbations depends on the tidal excursion parameter $\eta = U_0 k/\omega_0$, a non-dimensional ratio between the tidal advection distance and the topographic horizontal wavelength. When $\eta << 1$, then $\partial w'/\partial t >> U(t)\partial w'/\partial x$, a limit known as the **acoustic limit**, (Bell, 1975) which applies for most tidal amplitudes and topographic lengthscales in the ocean.

The full solution for w in the acoustic limit with constant N is $w = U_0 h_0 k cos(kx) cos(mz + \omega_0 t)$, giving upward energy flux, where the vertical mode number, m, satisfies the dispersion relation,

$$m = k\sqrt{\frac{N^2 - \omega^2}{\omega^2 - f^2}} \tag{25}$$

with $\omega = \omega_0$, and k given by the length-scale of the topography. The positive root ensures upward energy flux. These propagating internal tides (i.e. internal waves at the tidal frequency) are possible only if $f < \omega_0 < N$. In this $\eta << 1$ limit, there are no lee-waves.

Quasi-steady lee-wave solutions occur if $\eta >> 1$ when the perturbation equations reduce to the steady-state equations. If $\omega_0 < f$ (i.e. at latitudes above the critical latitude where $f = \omega_0$ for that tidal frequency) lee-waves will dominate the vertically propagating part of the solution if $f < U_0 k < N$.

Internal tide solutions are linear if $|u'/U_0| << 1$, which implies

$$\gamma = \frac{\text{topographic steepness}}{\text{wave characteristic steepness}} = \frac{h_0 k}{k/m} = \frac{h_0 k}{\sqrt{\frac{\omega^2 - f^2}{N^2 - \omega^2}}} << 1 \tag{26}$$

The linearity of the internal tide solutions is therefore dependent on the parameter γ, the relative steepness of the topography. Note that γ is not the same as the relative steepness in the steady lee-wave problem Fr_L, since the internal wave frequency in the oscillating flow problem is set by the tidal frequency.

The lee-wave Froude number Fr_L is nonetheless an important parameter even in the oscillating flow problem, since if $Fr_L > 1$, there will be topographic blocking of the flow at the maximum flow-speed of the oscillating tide (Winters & Armi, 2013). Moreover, $Fr_L \approx \gamma/\eta$, when $f << \omega_0 << N$, so large Fr_L implies steep topography and small relative excursion distance. This small η might suggest lee-waves are therefore not possible for large Fr_L. However, when there is blocking, both the effective height and width of the topography are modified: only the layer $h_{eff} = U_0/N$ below the top of the ridge moves over the topography, reducing the effective width of the topography to $h_{eff}/\alpha_t = (U_0/N)/\alpha_t$, where α_t is the aspect ratio (height/width) of the topography near the top. The resultant effective excursion parameter for the oscillating flow is then $\eta_{eff} = \alpha_t N/\omega_0 \approx \gamma$. Hence for steep topography, large Fr_L will produce a large effective η response, putting the waves in the quasi-steady lee-wave regime with blocking.

The relative steepness γ is also important in determining whether lee-waves will have time to develop in an oscillating flow (Klymak et al., 2010a). When a flow is initiated over topography, the lee-wave signal will take a time $t_L = \lambda_z/(c_{gz})$, to propagate one vertical wavelength λ_z above the topography, where c_{gz} is the vertical component of the group velocity. If $t_L >> \pi/\omega_0$, then the lee-wave signal will not become established before the flow reverses direction. In the limit of $f << U_0 k_{eff} << N$, $c_{gz} \approx N k_{eff}/m^2$, where k_{eff} is the effective horizontal wavenumber of the topography $k_{eff} \sim \alpha_t N/U_0$ for $Fr_L > 1$, and $m \approx N/U_0$ for a lee-wave. Hence $t_L \approx 2\pi/(N\alpha_t)$, and the tidally-driven lee-wave signal will only propagate at least one-vertical wavelength above the topography before the forcing flow switches direction if $t_L < \pi/\omega_0$, or $\alpha_t/(\omega_0/N) > 2$. Since $\alpha_t/(\omega_0/N) \approx \gamma$, (assuming $f << \omega_0 << N$), the topography must be steep for tidally-driven lee-wave development if $Fr_L > 1$. For $Fr_L < 1$, a similar argument, but with k set by the topographic wave number gives $\eta > 1$ for lee-wave development during the oscillation period.

For tidally-driven lee-waves, linear lee-waves with $Fr_L < 1$ occur when $\eta > 1$, while nonlinear lee-waves with $Fr_L > 1$ require both steep topography $\gamma > 1$ and large effective η. By comparison in steady flows nonlinear waves require only $Fr_L > 1$.

2.3 Nonlinearity and lee wave breaking at the generation site

While linear theory is helpful for understanding the mechanisms for lee-wave generation and the regimes in which lee-waves are possible, we must examine the nonlinear regimes to identify how lee-waves break and lead to mixing.

When Fr_L is increased, the effective height of the topography is reduced to $h_{eff} \sim U_0/N$ (Winters & Armi, 2012). Increasing the topographic height therefore leads to a saturation of the energy flux at or near $Nh_0/U_0 = 1$ (Nikurashin & Ferrari, 2010b). The saturation of the lee-wave energy flux occurs at lower values of Nh_0/U_0 for 2-dimensional topography than for 1-dimensional topography, as flow is forced around topographic crests, rather than over them (Nikurashin et al., 2014). This modification of the lee-wave energy conversion can be quantified by (Nikurashin & Ferrari, 2011)

$$C = C_{\text{linear}} \left(\frac{(Fr_L)c}{Fr_L} \right)^2 \tag{27}$$

where $(Fr_L)_c$ is the critical leewave Froude number $(Fr_L)_c = 0.7$ for 2D flows and 0.4 for 3D simulations with 2D topography (Nikurashin et al., 2014)). This is equivalent to calculating the energy flux from eqn 20 or 21 based on the effective height, rather than the actual height.

The existence of this saturation for $Nh_0/U_0 > Fr_{Lc}$ might suggest propagating waves of large enough amplitude to cause breaking (i.e. local Froude number > 1) cannot be generated, and breaking of waves will only occur if there is additional modification of the waves by the ambient conditions through which they propagate or instability mechanisms.

However, this only considers the propagating wave component of the solution. When blocking occurs, the flow at the topography takes on the form of an internal hydraulically controlled flow, with a jet of height U_0/N above the topography, which plunges below the crest of the topography on the lee-side, which may be the location of strong localized turbulence (Winters & Armi, 2012). Dependent on the downstream flow conditions (e.g. another topographic feature) the flow may be forced from this supercritical flow into a subcritical regime via an internal hydraulic jump, which again can be a location of strong turbulence (Winters, 2016). Lee-waves can still propagate above the hydraulic jump, provided the flow and stratification above this layer are conducive to their propagation. The fluctuations associated with the turbulent layer can themselves be the source of internal waves, often with frequencies greater than $U_0 k$, and closer to N (Aguilar & Sutherland, 2006). Understanding the mixing driven by stratified flow over topography requires examination of this hydraulic flow as well as the upwardly propagating lee-wave component.

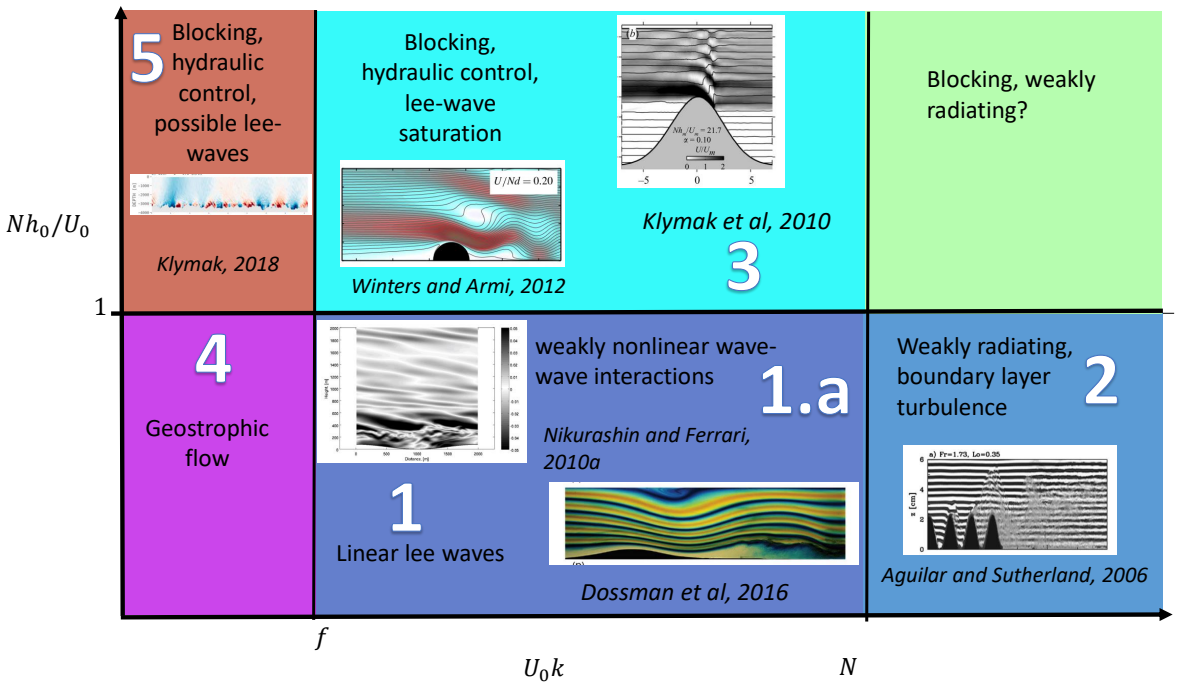

Figure 2: Regime diagram for lee-waves. Wave behavior depends on the non-dimensional parameters Nh_0/U_0, U_0k/f and U_0k/N. For the 6 regimes shown, examples of behavior from numerical simulation or laboratory experiments are shown as snapshot images. The numbers for each regime are used in the descriptions in the text.

We will now consider mixing as a function of the three nondimensional parameters, Fr_L, U_0k/f, U_0k/N (**Figure 2**). When $Fr_L < 1$, $f < U_0k < N$ (Regime 1 in **Figure 2**), this regime is characterized by linear propagating lee-waves. Mixing only results if the wave-energy is transferred to smaller scales such that the wave Froude number is increased, and/or Richardson numbers are decreased. Nikurashin & Ferrari (2010b) shows that for 2D sinusoidal topography, in the presence of rotation, in the weakly nonlinear regime of $0.3 < Fr_L < 0.7$ (Regime 1.a in **Figure 2**) a parametric instability transfers energy between the mean flow, lee-waves, and inertial oscillations, and the strong vertical shear associated with the inertial oscillations leads to wave breaking and mixing. For parameters corresponding to the Southern Ocean, about 50% of the radiated wave energy is dissipated in the bottom 1km (Nikurashin & Ferrari, 2010a). For lower values of Fr_L, the weakly nonlinear interaction does not occur, so linear lee-waves radiate upwards without breaking, while for larger values of Fr_L, the lee-wave generation saturates as described above. The weakly nonlinear theory used to explain these simulations relies on the presence of wave-damping due to the wave breaking. These numerical simulations may have excessive viscous damping, due to the limitations of the numerical resolution (Shakespeare & Hogg, 2017), in which case the wave-mean-flow interaction and bottom-enhanced dissipation may be over-emphasized.

In the $Fr_L < 1$, $U_0k > N$ regime (Regime 2 in **Figure 2**), where flow is not blocked, but radiating wave solutions are not possible, mixing takes place through bottom boundary layer turbulence (Dossmann et al., 2016) downstream of the topography, with the maximum mixing concentrated at the level of the topography. This turbulent region excites upward propagating internal waves with frequencies close to N (Aguilar & Sutherland, 2006).

When $Fr_L \geq 1$, $f < U_0k < N$, (Regime 3 in **Figure 2**) this regime is characterised by blocking, with generation of lee-waves of vertical lengthscale U_0/N above the topography, hydraulic control of the jet above the topographic crest, and the possibility for a stagnant wedge downstream of the crest, with mixing occurring primarily in the hydraulic jump downstream if present (Winters & Armi, 2012, Winters, 2016, Klymak et al., 2010a). Dossmann et al. (2016) measures small total mixing in this regime relative to the $Fr_L < 1$ regimes; but this comparison does not normalize for the varied mean flow kinetic energy. The vertical profile of mixing shows most mixing concentrated

in a thin layer near the topography, with very little mixing away from the topography. Winters & Armi (2014) show strong dissipation occurring in the internal hydraulic jump downstream of the topographic crest, with substantial turbulent fluctuations. The internal hydraulic jump depends on the downstream conditions (e.g. presence and height of another topographic feature). No radiating lee-waves are present in these simulations because the flow is confined to the narrow jet above the topography. (Aguilar & Sutherland, 2006) shows that the boundary layer separation downstream of the topographic crest, strongly linked to the vorticity source for turbulence in Winters & Armi (2014), is highly dependent on the shape of the topography.

The energy loss from the mean flow can be estimated from the work done by the form drag, where the form drag is given by

$$F_d = \int_{-\infty}^{+\infty} P_b \frac{dh}{dx} dx \tag{28}$$

where P_b is the pressure at the sea-floor and dh/dx is the topographic slope. When $Fr_L > 1$ and the flow is hydraulically controlled at the topography (**Figure 1b**), (Klymak et al., 2010a) suggests a simple hydrostatic model for the form drag . The stratified fluid is approximated by a 2.5 layer system, where the upper infinitely deep layer is the uncoupled flow a distance h_u above the topography (Winters & Armi, 2012). The lower layer is blocked upstream of the topography (where it has a depth equal to the height of the topography h_0), and the middle layer is the layer which is above the crest upstream, but displaced downwards downstream of the crest by a distance Δh. The density difference between the bottom and middle layers is related to the constant stratification N by $\Delta\rho = \rho_0 N^2(h_0 + h_u)/2g$. Assuming hydrostatic pressure, the form drag is then:

$$F_{h_0} = \int_{-h_0}^{-\Delta h} g\Delta\rho\Delta h dh + \int_{-\Delta h}^{0} g\Delta\rho h dh = \frac{\rho N^2}{2}\Delta h h_0^2 \left(1 + \frac{h_u}{h_0} - \frac{3}{2}\frac{\Delta h}{h_0} - \frac{3}{2}\frac{h_u}{h_0}\frac{\Delta h}{h_0}\right) \tag{29}$$

Both Δh and h_u are proportional to U_m/N where U_m is the flow speed at the crest. Based on numerical simulations, Klymak et al. (2010a) propose $\Delta h = \lambda_0/3$, and $h_u = \lambda_0$ where $\lambda_0 = 2\pi U_m/N$. The form drag then becomes:

$$F_{h_0} = \rho N U_m h_0^2 \frac{\pi}{2} \quad 1 + \pi\frac{U_m}{N h_0} - 2\pi^2\left(\frac{U_m}{N h_0}\right)^2\Bigg) \tag{30}$$

This hydrostatic prediction for the drag compares well with the drag diagnosed from 2D numerical simulations in the $Nh_0/U_0 >> 1$ regime (Klymak & Legg, 2010). For an infinitely deep fluid (where $U_m \approx U_0$, the barotropic forcing velocity) the total work per unit width done by the drag is then:

$$W = -F_{h_0}U_0 = \rho N U_0^2 h_0^2 \frac{\pi}{2} \quad 1 + \pi\frac{U_0}{N h_0} - 2\pi^2\left(\frac{U_0}{N h_0}\right)^2\Bigg) \approx \rho N U_0^2 h_0^2 \frac{\pi}{2} \text{ for large } Nh_0/U_0 \tag{31}$$

In steady state, this energy extracted from the mean flow can be transferred to dissipation and mixing, or to radiating internal waves (which may in turn lose energy to dissipation and mixing), or to larger scale flows (e.g. the flow opposing the mean flow which provides the blocking). Note that this is the total energy lost over a single bump. If we had a succession of bumps, separated by a distance $2\pi/k$, then the average energy conversion per unit area would be

$$C = W/(2\pi/k) = \frac{\rho N U_0^2 h_0^2 k}{4} \text{ for large } Nh_0/U_0 \tag{32}$$

Note the similarities to the energy conversion eqn 20. In particular note that despite being in the high Fr_L regime, this total energy conversion does not saturate (i.e. E continues to increase as h_0 increases), although it is half the magnitude of the linear prediction. This energy conversion includes both the energy conversion to the blocked upstream region and hydraulic jump, as well as the propagating lee-waves. The energy conversion from bottom flow to blocked flow does not necessarily contribute to mixing, so this energy conversion estimate does not tell us the energy which is available for mixing. Nonhydrostatic effects may further modify the bottom drag (Mayer in review).

For an estimate of the energy available for mixing by breaking propagating waves in the blocking regime, we could apply the lee-wave energy conversion formula (eqn 20) to only the top part of the topography, above the level of blocking. Then we obtain:

$$C = \frac{1}{2}\rho_0 U_0 h_{eff}^2 \sqrt{(U_0^2 k_{eff}^2 - f^2)}\sqrt{(N^2 - U_0^2 k_{eff}^2)} \tag{33}$$

which for $f << U_0 k_{eff} << N$ becomes

$$C = \frac{1}{2}\rho_0 U_0^2 k_{eff} h_{eff}^2 N \tag{34}$$

Note that this is not the same as the energy conversion estimate in eqn 27 because here both effective height and effective horizontal wavenumber are included, whereas 27 only uses the effective height, and assumes the topographic wavenumber determines the horizontal wavenumber, even after blocking. When blocking reduces the effective length scale of the topography sufficiently that $U_0 k_{eff} > N$, from Equation 33 propagating lee-waves are no longer possible and the lee wave energy conversion is zero, consistent with results of F. Mayer and O. Springer (in review).

If we write $h_{eff} k_{eff} = \alpha_t$ where α_t is the topographic aspect ratio at the top of the topography, and use $h_{eff} = 2\pi U_0/N$, then

$$C = \pi \rho_0 U_0^3 \alpha_t \tag{35}$$

If this component of the energy conversion is balanced by dissipation, then we would expect total dissipation to scale like U_0^3, as documented in Klymak & Legg (2010).

The $Fr_L < 1$, $U_0 k < f$ regime (Regime 4 in **Figure 2**) is characterized by geostrophic flow, and propagating lee-waves are not permitted. By contrast, if $U_0 k < f$ and $Fr_L > 1$, (Regime 5 in **Figure 2**) blocking reduces the effective height of the topography $h_{eff} = U_0/N$ and effective width, so that lee-waves are indeed possible if $k_{eff} = \alpha_t/h_{eff} > f/U_0$. Klymak (2018) estimates form drag using eqn 30 to estimate the energy loss for large-scale topography and compares with numerical simulations of rough, low-pass filtered topography (so $U_0 k < f$). The energy loss from the mean flow (and hence dissipation in steady state) scales like U_0^2 for large Fr_L, in agreement with predictions such as eqn 31. These simulations use a doubly-periodic domain, with a forced barotropic flow. The energy input required to force the blocked flow back to a barotropic state is balanced by the topographic energy conversion. In steady state, this energy conversion from the barotropic to the blocked flow is balanced by dissipation, which therefore scales like U_0^2, not U_0^3 as seen in simulations where the low modes can propagate out of the domain without dissipating (e.g. Klymak & Legg (2010)). Interestingly, including both large and small-scales of topography leads to higher dissipation than the sum of large-scale and small-scale simulations, suggesting that the hydraulic flows induced by the large-scale topography can enhance the wave radiation at the small-scale topography.

Tidally-driven transient lee-waves can be separated into two distinct regimes: when $\omega_0 > f$ so that the fundamental frequency internal tides are freely propagating, and when $\omega_0 < f$, so that the fundamental frequency internal tides do not propagate. In the first regime, the transient lee-waves are the result of the superposition of tidal harmonics into a beam (Musgrave et al., 2016b). The total dissipation in 2D simulations (Klymak et al., 2010b) is well-captured by a model which assumes the flow at the topographic crest arrests all internal tides with phase speeds less than or equal to the flow speed, and all the arrested waves dissipate locally:

$$D = \text{total dissipation} = \sum_{n_c}^{\infty} C_n \tag{36}$$

where C_n is the linear tidal energy conversion to internal tide vertical mode n, and n_c is the critical vertical mode above which the horizontal phase speed $c_n < U_m$, the flow speed above the topography (where $U_m \approx U_0$ for a deep ocean). This model gives a total dissipation which scales like U_0^3, since C_n scales like U_0^2 and the number of arrested modes scales like U_0. Simulations show the dissipation is concentrated near the top of the topography, with a decay scale proportional to U_0/N, implying that the transient arrested waves lead to local breaking (in contrast to the steady lee-wave problem, where lee-waves largely propagate upward without breaking). This implies that local breaking is greater in the time-dependent problem, perhaps a result of the temporal reversal of the barotropic flow.

For the second regime where $\omega_0 < f$, i.e. diurnal tides more than $\pm 30^\circ$ away from the equator, or semidiurnal tides at very high latitudes, there are no propagating internal tides. However, transient lee-waves and internal hydraulic jumps can still occur, sometimes in the presence of bottom-trapped horizontally propagating disturbances (Musgrave et al., 2016a, Nakamura et al., 2000). Like the steady flow scenario, much of the mixing may occur in the region of the flow separation and hydraulic jump downstream of the topographic crest, but above the topography breaking propagating lee waves also contribute to mixing (Musgrave et al., 2016a). A simple estimate of energy conversion in this oscillating flow regime assumes that quasi-steady linear lee-waves exist at any instant in time with energy conversion from eqn 20:

$$C(t) = \frac{\rho_0}{4\pi^2} \int_{-\infty}^{+\infty} \int_{-\infty}^{+\infty} \frac{\mathbf{U_0(t)}.\mathbf{k}}{|\mathbf{k}|} P(\mathbf{k}) \sqrt{(U_0(t)k^2 - f^2)} \sqrt{(N^2 - U_0(t)k^2)} d\mathbf{k} \tag{37}$$

with the time-averaged energy flux obtained from the integral of this instantaneous energy flux over a tidal cycle. For a sinusoidal 1-dimensional topography, and unidirectional oscillating flow $U_0 cos(\omega_0 t)$, in the limit of $f << U_0 k << N$ this gives:

$$C = \frac{1}{4}\rho_0 U_0^2 h_0^2 N k \tag{38}$$

or 1/2 the energy conversion from a steady flow of magnitude U_0 in the same $f << U_0 k << N$ limit.

2.4 Propagation and lee wave breaking remote from the generation site

Lee-waves can propagate both upward and downstream from the topographic generation site, and their ultimate breaking will lead to turbulent dissipation and mixing remote from the topography where they were generated. As lee-waves propagate away, they encounter changes in background conditions (flow and stratification) which can modify the wave properties such that an initially linear wave becomes nonlinear and breaks.

To demonstrate the impact of advection by the mean flow on the distribution of mixing due to lee-waves, Zheng & Nikurashin (2019) conduct numerical simulations of lee waves generated over rough topography and advected over flat topography downstream. In their simulations, about 50% of the dissipation occurs in the downstream flat topography region, where much of the lee-wave energy derives from downward reflection of upward propagating lee-waves at the upper boundary. Variable shear and stratification would modify this downward reflection.

We will now relax the assumption that N is constant, and instead examine the consequences of a stratification that varies with height. When lee-waves propagate into regions with variable flow and/or stratification, WKB theory can be used to estimate how the wave properties change along the wave characteristics, assuming the stratification and flow change slowly in the vertical relative to m^{-1}. From the dispersion relation

$$\omega_d(z) = \omega_s - U(z)k = \sqrt{\frac{N^2(z)(k^2+l^2) + f^2 m^2(z)}{k^2 + l^2 + m^2(z)}} \tag{39}$$

where ω_s is the frequency in the stationary frame, and $\omega_s - Uk$ is the Doppler shifted frequency ω_d. (Here k is the wave-number component in the horizontal direction aligned with the mean flow, while l is the horizontal wave-number component perpendicular to the mean flow). If we generate a stationary wave, so that $\omega_s = 0$, then as the wave radiates upward into a different region with different flow and stratification, the Doppler shifted frequency and vertical mode number will both change:

$$m^2(z) = \frac{(N^2(z) - U^2(z)k^2)}{(U^2(z)k^2 - f^2)}k^2 \tag{40}$$

If $U(z)$ increases toward N/k (i.e. due to an increase in flow speed or a decrease in stratification), then $m \to 0$, when the wave energy will be reflected downward from this turning level. Wave amplitude can be increased by trapping in a waveguide region below a turning level (Scorer, 1949).

If $U(z)$ reduces toward f/k, then m becomes very large, wavelengths become small, increasing shear in the wave, and reducing the vertical component of group velocity $\partial\omega_d/\partial m$. At this critical layer (Booker & Bretherton, 1967), the wave energy can no longer propagate upward. For small Richardson numbers instability and wave breaking can occur (Winters & Riley, 1992), while for large Richardson numbers, the wave energy can be absorbed by the mean flow (Booker & Bretherton, 1967). Kunze & Lien (2019) shows that a fraction of the wave energy up to $(kU_0 - f)/kU_0$ can be reabsorbed by the mean flow, where U_0 is the flow speed at the generation site. A greater fraction of high frequency lee-wave energy will be reabsorbed than near-inertial lee-wave energy. This reabsorption therefore influences the energy remaining for dissipation and mixing.

Lee waves can also encounter turning latitudes when they propagate poleward such that $f > \omega_d$, refracting the wave-energy back toward the equator. The dependence of lee-wave properties on environmental properties (stratification, flow, coriolis) suggests that unlike low-mode internal tides, lee-waves do not propagate far away from their generation site.

2.5 Summary of key predictions from theory, laboratory and numerical simulation

Energy conversion from the mean-flow gives an upper bound for the energy which can be used for mixing. For linear waves (i.e. $Fr_L < 1$) eqns 20, 21 indicate the dependence of lee-wave energy input on bottom stratification, bottom

flow speed and topographic roughness. This energy conversion is expected to be reduced for steep topography (i.e. $Fr_L \geq 1$) following eqns 27 or 33. For $Fr_L > 1$, more of the energy conversion may contribute to the upstream blocking and downstream hydraulic jump. While the former will not lead to local mixing, the latter is a site of local mixing. Separating the energy conversion to propagating lee-waves and non-propagating components is a complicated, incompletely understood problem. Linear theory suggests energy conversion only occurs for $f < U_0 k < N$. However, numerical simulations and laboratory experiments show that outside these limits, energy is still extracted from the mean flow and used for mixing, in hydraulic jumps or bottom boundary layers. Lee-waves can also be generated outside the $f < U_0 k < N$ limit if the effective vertical and horizontal scales of the topography are reduced by blocking.

The vertical wavenumber of lee-waves, eqn 15, is dependent on the intrinsic frequency, stratification and rotation. As waves move into regions of different flow and stratification, the vertical wave number is modified, leading to critical layers when vertical wave number approaches infinity. Critical layers are potential locations of enhanced mixing, or energy reabsorption by the subinertial flow.

3 OBSERVATIONS OF OCEANIC LEE WAVES AND MIXING

Lee-waves driven by slowly varying flow are difficult to observe in the ocean, since they are stationary in the frame of the topography, are generated at deep bottom topography where measurements are challenging, and are often generated by a chaotic time-evolving mesoscale eddy field. Much of the evidence for lee-wave driven mixing is therefore circumstantial: associating enhanced levels of mixing with the conditions predicted to give large energy input into the lee-wave field (i.e. rough topography at around the right length-scales, significant bottom velocities over that topography). Tidally-driven lee-waves are more readily accessible, given the greater predictability of the forcing flow, and the presence of strong tidal currents across relatively shallow topography such as in coastal regions and submarine ocean ridges.

3.1 Observational diagnostics for lee-waves and mixing

Three different methods are used to estimate mixing in the stratified ocean. (a) Tracer release experiments provide direct estimates of tracer diffusivity (Watson et al., 2013). (b) Velocity microstructure provides estimates of kinetic energy dissipation ϵ

$$\epsilon = 15 \left(\frac{\nu}{2}\right) \left(\frac{\partial u}{\partial z}\right)^2 \tag{41}$$

(where ν is the molecular viscosity, u is the horizontal velocity and z is the vertical coordinate), which are related to diapycnal diffusivity κ through the Osborn (1980) relation:

$$\kappa = \Gamma \epsilon / N^2 \tag{42}$$

where Γ is the mixing efficiency, assumed to be a constant 0.2. (c) Dissipation is estimated from vertical profiles of density and velocity using a fine structure parameterization, (Henyey et al., 1986, Wijesekera et al., 1993, Gregg, 1989, Gregg et al., 2003) :

$$\epsilon = \epsilon_0 \frac{< V_z^2 > / \overline{N}^2}{< V_{z_{GM}}^2 > / N_0^2} L(f, f_0, N, N_0) h(R_\omega) \tag{43}$$

where $\overline{N}$ is an average stratification, ϵ_0 is the background turbulent dissipation of the Garrett-Munk (GM) spectrum, f_0 is the GM reference value of Coriolis, and N_0 is the GM reference stratification. $< V_z^2 > / \overline{N}^2$ is the shear variance (deduced from the fourier transform of the vertical profile and integrated over a wavenumber band appropriate for internal waves), normalized by the average stratification, and $< V_{GM}^2 > / N_0^2$ is the normalized shear variance for the GM spectrum at the reference stratification. The function $L(f, f_0, N, N_0)$ accounts for latitude and stratification, and R_ω is the shear-to-strain ratio:

$$R_\omega = \frac{V_z^2}{\overline{N}^2 \zeta_z^2} \tag{44}$$

where $\zeta_z = (N^2 - N^2_{ref})/N^2_{ref}$ is the strain and N^2_{ref} is the background stratification corresponding to an adiabatically adjusted density profile. For a single wave, R_ω is related to the Doppler shifted frequency ω_d:

$$R_\omega = \frac{(\omega_d^2 + f^2)(N^2 - \omega_d^2)}{N^2(\omega_d^2 - f^2)} \approx \frac{(\omega_d^2 + f^2)}{(\omega_d^2 - f^2)} \tag{45}$$

(Polzin 1995), so that the function h is therefore largely a function of wave frequency. Waterman et al. (2013), Meyer et al. (2015) provide more details of the use of the fine structure parameterization and shear variance in the context of Southern Ocean lee-waves. **Figure 3** and **Figure 4** show several examples of dissipation observations associated with lee-waves driven by geostrophic and tidal flow respectively.

Whereas the microstructure estimate is a direct estimate of dissipation, assuming only isotropy and homogeneity, the fine-structure parameterization assumes that a Garrett-Munk-like internal wave spectrum leads to mixing through a cascade of energy to small-scales. These assumptions may not apply near internal wave generation sites, or in regions where internal wave energy is reabsorbed by the geostrophic flow.

Internal wave energy can be estimated from vertical profiles of velocity and density:

$$E_{\text{Iwave}} = \frac{1}{2}(< u^2 > + < v^2 >) + \frac{1}{2}\overline{N}^2 < \eta^2 > = E_{KE} + E_{PE} \tag{46}$$

u and v are the perturbation horizontal velocity components, and η is the vertical displacement. The perturbation quantities are deduced from the fourier transforms of the vertical profiles, integrated over the wavenumber band appropriate to internal waves (Waterman et al., 2014).

The vertical direction of energy propagation can be deduced from the ratio of the counterclockwise to clockwise polarized shear variance, integrated over the internal wave vertical wavenumber band. In the Southern hemisphere, predominantly clockwise polarized shear indicates predominantly upward internal wave energy flux. (Waterman et al., 2013, Meyer et al., 2015, Gonella, 1972).

The dominant intrinsic frequency of the perturbations is deduced from R_ω, and the wavelength of perturbations is deduced from the separation between coherent maxima or from the peaks in vertical wavenumber spectra.

3.2 Lee waves generated by subinertial flow

Much of the observational evidence for mixing by lee-waves driven by geostrophic flow comes from the Southern ocean, where the strong bottom velocities associated with the Antarctic Circumpolar Current interact with abyssal topography on the small scales required for lee-wave generation (eqn 16).

Enhanced dissipation associated with rough topography and strong near-bottom currents has been found from application of the fine-structure parameterization (eqn 43 or variants) to hydrographic profiles in the Southern ocean (Sloyan, 2005), including in the Drake Passage (St. Laurent et al., 2012, Sheen et al., 2013), a region of relatively steep topography ($Fr_L \sim 0.7$) and strong ACC frontal velocities. A year-long record from moorings in a region of the Drake Passage where the SubAntarctic Front encounters rough topography (Brearley et al., 2013) shows that enhanced inferred dissipation is associated with strong subinertial bottom currents. Microstructure measurements (eqn 41) across Drake Passage St. Laurent et al. (2012), Sheen et al. (2013) (**Figure 3a**) confirm bottom-enhanced dissipation associated with the strong velocities of the ACC frontal regions at locations of rough topography such as the Phoenix Ridge, consistent with enhanced diffusivities measured in this region by tracer release (Watson et al., 2013).

Evidence for the role of bottom generated internal waves in generating this dissipation comes from the upward propagation of wave energy indicated from velocity rotary spectra (St. Laurent et al., 2012, Sheen et al., 2013, Brearley et al., 2013); vertical wavelengths deduced from shear spectra which are consistent with linear predictions of 300-1000m, given typical flow speeds, stratification, and topographic length-scales (St. Laurent et al., 2012, Sheen et al., 2013); and enhancement of internal wave kinetic energy (eqn 46) at both near-inertial and higher frequencies when bottom currents are strong (Brearley et al., 2013).

There is however a mismatch between the measured dissipation and the lee-wave energy flux estimated from linear theory (e.g. eqn 21). Brearley et al. (2013) finds the total dissipation in the bottom 900m is only 21% of the predicted lee-wave energy flux. Sheen et al. (2013) shows a similar ratio ($10 - 30\%$) between measured dissipation and linear theory predictions of radiated lee-wave energy, which might in part result from a loss of wave energy to the mean flow, suggested by an overestimate of turbulent dissipation rates by finescale parameterizations (eqn 43). The fraction of energy dissipated in the bottom 1-km increases with topographic steepness, in line with nonlinear predictions of

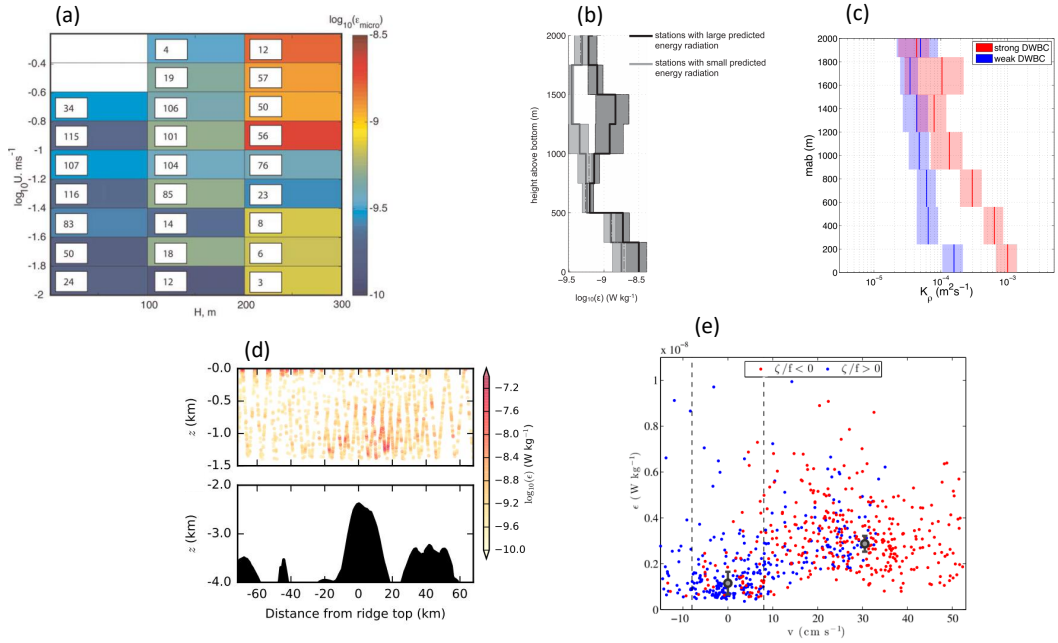

Figure 3: Observations of mixing by lee-waves generated by geostrophic flow. (a) Dissipation ϵ as a function of bottom roughness height H and bottom flow speed U in the Drake Passage, from Sheen et al. (2013); (b) Mean dissipation profiles for regions with large and small predicted lee-wave energy (from linear theory) in Kerguelen Plateau region of the Southern Ocean, from Waterman et al. (2013); (c) Mean dissipation in the Deep Western Boundary Current, for periods of strong and weak bottom current, from Köhler et al. (2014); (d) Dissipation from profiling floats in a lee-wave in the Drake Passage from Cusack et al. (2017); (e) Dissipation in mesoscale eddies on the western boundary from Clément et al. (2016).

Nikurashin & Ferrari (2010b). Direct measurements of vertical energy flux $< w'p' >$ in a topographic lee-wave were made by profiling floats crossing the Shackleton Fracture Zone in the Drake Passage (Cusack et al., 2017). In this case linear predictions suggest an evanescent response, in the $U_0 k < f$ regime. However, if the reduction in effective height and wavelength of the topography by the effect of blocking $Fr_L > 1$ is taken into account, the upward energy flux magnitude is consistent with theoretical predictions (e.g. eqn 33). The depth-integrated dissipation (**Figure 3d**) is about two orders of magnitude smaller than this energy flux.

In addition to the Drake Passage region of the Southern Ocean, the region around the Kerguelen Plateau, in the South Indian Ocean, is another location where the main fronts of the ACC encounter rough topography. Whereas the Drake Passage topography reaches steepness of $Fr_L = 0.7$, the topography near the Kerguelen Plateau is less steep, at about 0.1. Observed signatures of lee-waves include enhanced near-bottom dissipation in some regions of large topographic roughness and large near-bottom flow speeds co-located with enhanced near-bottom internal wave energy and upward wave energy propagation (Waterman et al., 2013, Meyer et al., 2015, 2016). The dissipation measured in the bottom 1000m is found to be $2 - 20\%$ of the internal wave energy radiation predicted from linear theory, a smaller percentage than in the Drake Passage, consistent with more linear waves generated in a region of less steep topography. Sinks for the internal wave energy include a possible critical layer suggested by enhanced dissipation about 1250-1500m above the bottom (**Figure 3b**); wave-mean flow interactions, indicated by a mismatch between finescale parameterization dissipation estimates and microstructure (Waterman et al., 2014); and downstream propagation implied by internal wave propagation speed deduced from profiling floats (Meyer et al., 2016).

Other significant regions of ocean lee-wave generation outside the Southern Ocean include the Deep Western Boundary Currents (DWBC), where strong bottom velocities encounter small-scale topographic variations. Two moorings at 16°N on the western continental slope of the North Atlantic (Köhler et al., 2014) resolve variations in

the DWBC, as well as internal waves. Bottom enhanced mixing deduced from the fine-structure parameterization applied to CTD and LADCP profiles during the same period are correlated with the presence of the DWBC (**Figure 3c**). While moored velocity spectra show a peak at the M2 tidal frequency, suggesting tidally-driven internal waves, an increase in near-inertial wave energy for strong DWBC may be evidence for the triad interaction mechanism described in Nikurashin & Ferrari (2010b).

Higher up the continental slope, the Western Boundary Currents can generate lee-waves over small-scale topography such as the Charleston Bump (de Marez et al., 2020). Mesoscale eddies generated by instability of the upper ocean western boundary currents can encounter topography as they propagate Westwards into shallower water. Anticyclonic eddies, with strong bottom velocities, identified from altimetry and moorings at 26.5°N in the Western North Atlantic (Clément et al., 2016) are associated with enhanced high frequency shear and upward group velocity, whereas no clear energy propagation direction is seen associated with surface intensified cyclonic eddies. Bottom enhanced kinetic energy in high-frequency and near-inertial wavebands in anticyclones may be associated with the upstream presence of a 300m topographic rise. The characteristics of the topography suggest that the flow is partially blocked, with lee-wave generation at the top of the rise. Fine-structure estimates of dissipation rate are enhanced for larger bottom flow (**Figure 3e**).

In addition to the Southern Ocean and western boundary currents, other locations where substantial subinertial bottom flow encounters variable bathymetry include flows over the rough topography of mid-ocean ridges, such as fracture-zone sills. Such flows may undergo mixing localized at canyon-spanning sills (Thurnherr et al., 2005, Thurnherr & St. Laurent, 2011, Liang & Thurnherr, 2012, Clément et al., 2017), associated with upward propagating internal wave energy.

Observations of the eventual dissipation of lee-waves away from the topographic generation sites are sparse. (Sheen et al., 2015) examines both the internal wave field (from rotary spectra and shear-strain ratios, eqn 44) and the dissipation (from microstructure, eqn 41) in a region of the Drake Passage in the presence of a mid-depth eddy, and again when the eddy is absent. The eddy is found to modulate both the dissipation and the internal wave characteristics: dissipation is suppressed within the eddy core and enhanced around the top and bottom boundaries of the eddy; upward propagating internal wave energy is suppressed above the eddy, and downward propagating internal wave energy is enhanced below the eddy. Internal wave frequencies are highest in the eddy core, and near-inertial on the eddy's upper and lower boundaries. A simple WKB ray-tracing model, assuming a single initial wave frequency, shows that the weak stratification of the eddy core could lead to reflection of upward propagating internal waves, while critical layer dissipation may be present above and below the eddy core. The mid-depth dissipation maximum noted by Waterman et al. (2013) is further evidence for critical layer dissipation of internal waves.

3.3 Lee waves generated by oscillating flow

Lee-waves generated by oscillating tidal flow over topography have been observed in greater detail than lee-waves driven by geostrophic flow, in part due to the greater predictability of the tides, and the presence of strong tidal currents across relatively shallow topography such as in coastal regions and submarine ocean ridges (Klymak & Gregg, 2003, Konyaev et al., 1995). In locations where the dominant tidal frequency is superinertial (e.g. equatorward of 74.28° for the M2 tide and equatorward of 30° for the K1 tide) lee-waves may coexist with freely propagating waves at the forcing frequency.

Tidal lee-wave observations complement observations of lee-waves driven by slowly-varying mesoscale flows by providing evidence for mixing in downstream hydraulic jumps when $Nh_0/U_0 > 1$, such as at Knight inlet (Klymak & Gregg, 2003, Farmer & Armi, 1999), the Mascarene ridge in the Indian Ocean (Konyaev et al., 1995, da Silva et al., 2011) and Mendocino escarpment (Musgrave et al., 2016a, 2017). The mode number of the internal hydraulic jump varies from location to location, with a mode 1 disturbance at Knight inlet, mode-2 at the Mascarene ridge, and higher mode at the Kaena ridge of the Hawaiian seamount chain. In these regions where lee-waves are generated by superinertial tides (i.e. $\omega > f$ where ω is the tidal frequency, and f is the coriolis frequency), the vertical mode number of the lee-wave can be interpreted in terms of the arrest of the internal tides, with increasing tidal flow leading to the arrest of progressively lower internal modes (Klymak et al., 2010b).

Tidally-driven hydraulic jumps are locations of enhanced mixing. At Knight inlet acoustic backscatter indicates turbulent mixing at the interface between the strong flow above the topography and the stagnant layer above. At Kaena ridge, strong turbulent dissipation is observed near the bottom, near the ridge crest, associated with tidally-driven overturns (Klymak et al., 2008) (**Figure 4a**). These overturns, of order 100m, are associated with high strain, rather than high shear, and so result from convective breaking of nonlinear tidal lee-waves (Klymak et al., 2008),

Figure 4: Observations of mixing by tidally-generated lee-waves. (a) Time-depth plot of dissipation and density (black contours) at Kaena ridge from Klymak et al. (2008); (b) Time-depth plot of dissipation and density (black contours) from Musgrave et al. (2016a).

consistent with numerical simulations (Legg & Klymak, 2008). Repeated underway CTD sections (Alford et al., 2014) show that at ebb tide, isopycnals are depressed to the lee of the topographic sill, and as the tide slackens, this lee-wave propagates up and over the sill. At Mendocino escarpment enhanced dissipation in the hydraulic jump and lee-wave occurs on a diurnal rather than semi-diurnal timescale (Musgrave et al., 2016a) (**Figure 4b**), as the subinertial diurnal tides generate a bottom-trapped wave which reinforces the flow through a channel in the ridge. Turbulence associated with the tidally-driven lee-wave extends along the lee-wave characteristic up to the surface, while turbulence associated with the hydraulic jump is confined to the ridge flanks.

The relative fraction of the baroclinic energy dissipated in the transient lee-wave depends on the relative fraction of energy in the lee-wave compared to the propagating lower mode internal tides. At Kaena ridge dissipation in the lee-wave scales like U_0^3, and forms a small fraction of the total energy converted from the barotropic to baroclinic tide, with most of the internal tide energy radiated away in low-modes (Klymak et al., 2008), while at the Luzon Straits double ridge system (Alford et al., 2015) about 40% of the energy converted from the barotropic tide at the ridge system is dissipated and used for mixing locally. At Mendocino escarpment (Musgrave et al., 2017) the local dissipation is estimated to account for about 28% of the total energy converted from the baroclinic tide. Unlike the Kaena ridge, where local dissipation scales like U_0^3, (Klymak et al., 2008), at the Mendocino escarpment the local dissipation scales like U_0^2, perhaps a consequence of the multi-frequency tidal flow and three-dimensional topography.

Enhanced dissipation associated with tidally-driven lee-waves is not confined to tall steep ridges, but also occurs at small-scale steep topographic features in the Mid-Atlantic Ridge (Dale & Inall, 2015). The relaxation of the tidal flow releases the arrested lee-waves and the internal hydraulic jumps propagate laterally as nonlinear dense bores associated with overturning and enhanced dissipation. While the net dissipation is only modestly larger than background levels, such small-scale tidal lee-waves may be more widespread than the large features seen over tall ridges.

Above the critical latitude for the M2 tide (74.28°), no propagating internal tides are possible, and so only transient lee-waves can be generated by the tidal flow. Rippeth et al. (2015) shows that dissipation in the Arctic is enhanced over sloping topography, and this enhanced dissipation correlates with energy loss from the barotropic tide. Rippeth et al. (2017) shows bottom enhanced dissipation is found correlated with the tidal cycle in a region of sloping topography above the critical latitude, suggesting tidally-driven lee-waves.

In summary, observations of tidally-driven lee-waves complement those of lee-waves generated by subinertial flow by providing more detailed evidence for localized mixing in hydraulic jumps and near-bottom bores.

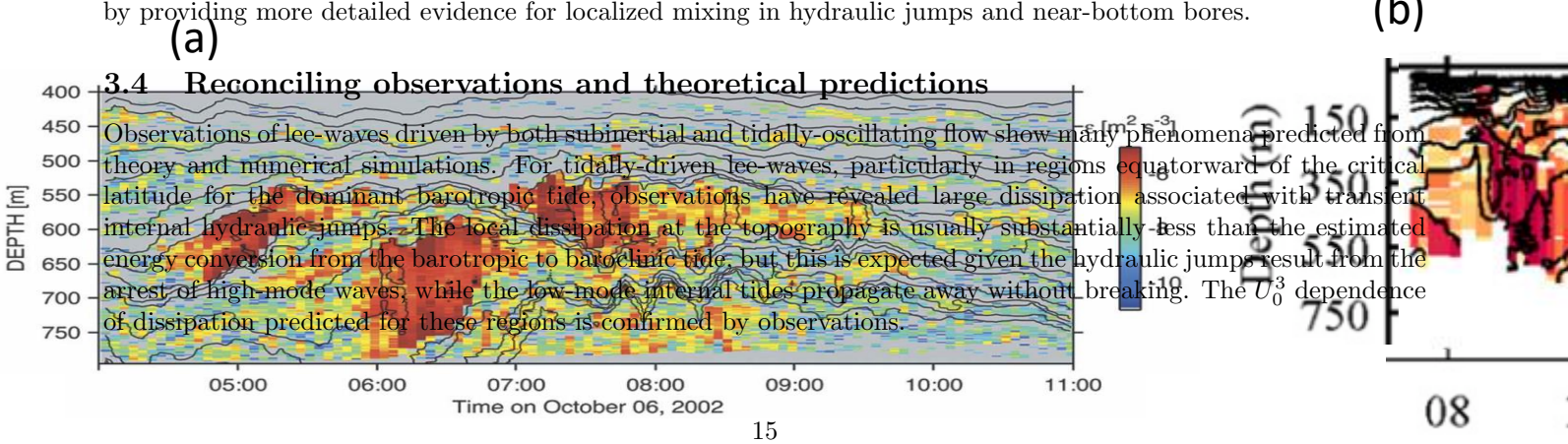

3.4 Reconciling observations and theoretical predictions

Observations of lee-waves driven by both subinertial and tidally-oscillating flow show many phenomena predicted from theory and numerical simulations. For tidally-driven lee-waves, particularly in regions equatorward of the critical latitude for the dominant barotropic tide, observations have revealed large dissipation associated with transient internal hydraulic jumps. The local dissipation at the topography is usually substantially less than the estimated energy conversion from the barotropic to baroclinic tide, but this is expected given the hydraulic jumps result from the arrest of high-mode waves, while the low-mode internal tides propagate away without breaking. The U_0^3 dependence of dissipation predicted for these regions is confirmed by observations.

By contrast to tidally-driven lee-waves, few direct observations exist of the details of nonlinear lee-waves and hydraulic jumps driven by mesoscale-eddy interaction with topography, due to the unpredictability of the driving flow. Observations confirm bottom-enhanced dissipation when bottom flows encounter rough topography, in both the Southern Ocean and on Western boundaries of ocean basins. Rotary shear spectra indicate upward energy fluxes, consistent with internal waves generated at topography. The net dissipation is however smaller than expected from the linear theory. This discrepancy may result from (a) the steepness of the topography (eqn 27); (b) the three-dimensionality of the topography, which reduces the predicted energy conversion (Nikurashin et al., 2014); (c) downstream advection of lee-waves, leading to dissipation far from the topography (Zheng & Nikurashin, 2019, Meyer et al., 2016); (d) the lack of observations near the bottom in the lee of large topographic features, where much of the energy converted from the barotropic flow may be dissipated in hydraulic jumps; (e) the transfer of lee-wave energy to the mean-flow through wave-mean flow interaction (Kunze & Lien, 2019); (f) the lack of sampling in critical layers associated with transient mesoscale eddies (Sheen et al., 2015).

4 PARAMETERIZATION OF MIXING BY OCEANIC LEE WAVES

If lee-waves break, they can contribute to irreversible mixing of the stably-stratified ocean interior, as shown numerically, experimentally and observationally (Nikurashin & Ferrari, 2010b, Aguilar & Sutherland, 2006). The scales at which the irreversible changes in density occur are much smaller than the scales of the waves themselves, and hence some numerical models may resolve the waves, but need to parameterize the mixing that results from the wave breaking. For such a model, which resolves the topography and the vertical and horizontal scales of the lee-waves, mixing can be parameterized by evaluating when the nonlinear lee-wave produces overturned isopycnals and convective instability. Klymak & Legg (2010) diagnoses the length scale of simulated buoyancy overturns associated with the breaking wave. The dissipation can be estimated by assuming this overturn length-scale is equivalent to the Ozmidov scale $L_O = (\epsilon/N^2)^{1/2}$. The tracer diffusivity is then estimated from the Osborn (1980) model (eqn 42).

In contrast to these wave-resolving models, the coarse resolution models used for climate simulations do not resolve the lee-waves, or the topography on the small-scales at which lee-waves are generated. Parameterizations of lee-wave mixing suitable for climate models connect the estimated energy conversion from subinertial flow over unresolved topography to the dissipation and mixing in the water column above. These parameterizations begin with an estimate of the energy conversion, such as the linear prediction in eqn 21, which after a rotation of horizontal coordinates so that the $\mathbf{U_0}$ vector is aligned with the topographic wavenumber $\mathbf{k}$ becomes:

$$C = \frac{\rho_0 |\mathbf{U_0}|}{2\pi} \int\!\!\!\int_{f/|\mathbf{U_0}|}^{N/|\mathbf{U_0}|} P_*(k) dk \sqrt{|\mathbf{U_0}|^2 k^2 - f^2} \sqrt{N^2 - |\mathbf{U_0}|^2 k^2} dk \tag{47}$$

where

$$P_*(k) = \frac{1}{2\pi} \int\!\!\!\int_{-\infty}^{+\infty} \frac{|k|}{|\mathbf{k}|} P(\mathbf{k}) dl \tag{48}$$

(Nikurashin & Ferrari, 2011).

This linear prediction for the energy conversion can be estimated given suitable values for the topographic spectrum $P(\mathbf{k})$, the bottom stratification N and the bottom velocity field $\mathbf{U_0}$. The estimate is complicated by the fact that the relevant velocity field, e.g. due to mesoscale eddies, may be poorly resolved at typical global model resolution, and the topography is not accurately known at the relevant small scales $\lambda < 2\pi U_0/f$. Choices therefore have to be made for the estimate of bottom velocity and topographic spectrum.

In Nikurashin & Ferrari (2011) the topographic spectrum is estimated by fitting an isotropic form of the Goff & Jordan (1988) spectrum

$$P_*(k) = P_0 k^{-\mu+1} \frac{B[1/2, (\mu-1)/2]}{B[1/2, \mu/2]} \tag{49}$$

(where B is the beta function) to single beam bathymetry soundings to determine P_0 and μ. The bottom stratification N is computed from the WOCE hydrographic atlas (Gouretski & Koltermann, 2004), and the bottom velocity is taken from a global ocean simulation at $1/8^\circ$ using the GFDL isopycnal model (Adcroft et al., 2010), averaging over 3 years of 5 day snapshots. The saturation of energy conversion at steep topography is accounted for by scaling E by a factor $(Fr_L/(Fr_L)_c)^2$ for $Fr_L > (Fr_L)_c$, where Fr_L is the lee-wave Froude number Nh_0/U_0, and $(Fr_L)_c = 0.7$.

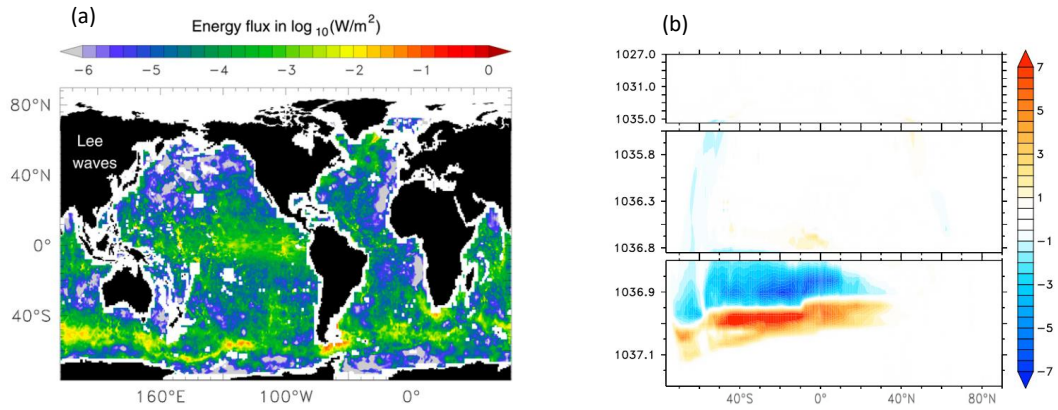

Figure 5: Global parameterization of lee-wave driven mixing and its impact: (a) Estimate of lee-wave energy conversion applied in a global climate simulation by Melet et al. (2014) after Nikurashin & Ferrari (2011); (b) The change in the overturning circulation in density space (Svedrups) resulting from including this lee-wave driven mixing estimate, from Melet et al. (2014).

The total global energy conversion rate to lee-waves is $0.2TW$, of which about half occurs in the Southern Ocean (**Figure 5a**).

A similar global estimate by Scott et al. (2011) used two independent topographic data sets, both following the Goff & Jordan (1988) stochastic model, (Goff & Arbic, 2010, Goff, 2010). The buoyancy frequency was derived from the WOA2009, and annually averaged, while bottom velocity estimates are taken from 1/12° simulations of the HYCOM model. The saturation of energy conversion at large steepness is included by scaling by a factor $\frac{1}{\pi}(Fr_L/Fr_{L_c})(arccos(1-2Fr_L/Fr_{L_c}) - 2(1-2Fr_L/Fr_{L_c})\sqrt{Fr_L/Fr_{L_c}(1-Fr_L/Fr_{L_c})})$ for $Fr_L > Fr_{L_c}$ (Welch et al., 2001), where $Fr_{L_c} = 0.75$ (in practice very similar to the saturation effect assumed in Nikurashin & Ferrari (2011)). In contrast to Nikurashin & Ferrari (2011), topography is not assumed to be isotropic. The resulting global energy conversion to lee-waves is about $0.44TW$ using the G2010 topographic dataset, and $0.34TW$ using the GA2010 dataset, somewhat greater that the (Nikurashin & Ferrari, 2011) estimate. The effect of steep topography was shown to be relatively small, accounting for only about 10% reduction in the global estimate. These energy conversion estimates from Scott et al. (2011) are considerably greater than the $0.22TW$ estimate of eddy energy loss (which could be attribted to energy conversion to lee-waves) made by Zhai et al. (2010) from altimetry and WOCE climatology.

Wright et al. (2014) perform a similar global estimate to Scott et al. (2011), using the G2010 topographic dataset and WOA2009-derived climatological bottom stratification, but with different bottom current estimates. Here values from the global 1/12° HYCOM simulation are combined with current meter observations using a model-assisted hierarchical clustering methodology. No correction for saturation at steep topography is included. The global estimate for energy conversion to lee-waves is $0.75TW$, considerably larger than Scott et al. (2011), and in agreement with the suggestion from Scott et al. (2011) that HYCOM underestimates bottom velocites by a factor of 2.

Most recently, Yang et al. (2018) uses all three previously used topographic data sets (e.g. GA2010, G2010, Nikurashin & Ferrari (2011)) and the output from the 1/10° GFDL CM2.6 global ocean simulation for the bottom velocities and bottom stratification to calculate the energy conversion to lee waves in the Southern Ocean only. The energy conversion is assumed to saturate for relative steepness greater than $Fr_{L_c} = 0.4$, consistent with 3D simulations from Nikurashin et al. (2014), and less than the saturation steepness values used in Nikurashin & Ferrari (2011) and Scott et al. (2011). The total energy conversion rates range from $0.10 \rightarrow 0.16TW$ for the different topography datasets, of which between $24-30\%$ is due to the time-mean flow and the reminder due to the eddy component of the flow. Increasing the value of steepness for saturation to 0.75 as in Scott et al. (2011) leads to a $1.5\times$ increase in energy conversion. Anisotropic topography is also shown to have a substantial (i.e. up to $\pm 100\%$) impact on the local rate of conversion.

All of these estimates of the energy conversion into lee-waves produce 2-dimensional spatial maps, which are constant in time. A full parameterization, enabling examination of the changes in lee-wave driven mixing in a changing climate, needs to include temporal variability due to changing bottom velocities and stratification. For

an eddy-resolving climate model, the instantaneous bottom velocity and stratification could be used. For non-eddy resolving models, the model's mesoscale eddy parameterization can provide estimates of eddy-velocities. Melet et al. (2015) uses the Mesoscale Eddy Kinetic Energy (MEKE) parameterization (Marshall & Adcroft, 2010, Eden & Greatbatch, 2008) to estimate the bottom velocity $\mathbf{U} = \alpha \mathbf{U}_E$, where $\alpha = 0.1$, and the mesoscale eddy velocity $U_E = \sqrt{2E}$, where E is the mesoscale eddy kinetic energy. Simulations of the GFDL CM2G model with the CMIP5 anthropogenic radiative forcing scenarios are used to obtain predictions of changing resolved and eddy velocities, and bottom stratification, while the topography and choice of saturation steepness follow the choices of Nikurashin & Ferrari (2011). Whereas in the present climate, energy conversion to lee waves is between $0.24 - 0.32TW$, under anthropogenic radiative forcing scenarios this is reduced by up to 26%. Possible feedbacks of this change in energy conversion on dependent parameters such as mixing and subsequent impacts on the climate model-simulated stratification and velocities are not however considered.

Estimating the energy conversion from subinertial flow to lee-waves is only the first step in parameterizing mixing, for which we want a temporally varying 3D spatial map of diffusivity. A common approach has been to follow the lead of tidal mixing parameterizations (e.g. St. Laurent et al. (2002)) and assume some fixed fraction of the energy conversion is dissipated "locally" (i.e. in the same horizontal location) and assume a particular vertical profile for that dissipation. Dissipation is then related to diffusivity using the Osborn (1980) model. i.e.

$$\kappa_d = \frac{\Gamma}{N^2} \frac{q_L C(x,y)}{\rho_0} F(z) \tag{50}$$

where κ_d is the diapycnal diffusivity, Γ is the mixing efficiency, N is the local stratification, q_L is the fraction of the lee-wave energy dissipated locally, $F(z)$ is the vertical structure function, and $C(x,y)$ is the lee wave energy conversion (e.g. eqn 47).

Currently, estimates of q_L range from 0.5 in 2D numerical simulations (Nikurashin & Ferrari, 2010b) to 0.1 in observations (Waterman et al., 2013), but there is little understanding of the factors that influence this variability. We have very little guidance for choice of the vertical distribution $F(z)$. Studies such as (Melet et al., 2014), (de Lavergne et al., 2016) and (Saenko et al., 2012) have therefore usually prescribed the same values of q_L between 0.3 and 1.0, and exponential form of $F(z)$ as used in tidal mixing parameterizations:

$$F(z) = \frac{e^{-z/\zeta}}{\zeta(1 - e^{-H/\zeta})} \tag{51}$$

where z is the height above bottom, H is the total depth and ζ is a fixed decay scale. The justification for constant q_L and exponential decay with a fixed decay scale is even weaker for the lee-wave problem than for the tidally-driven mixing problem.

Given this assumed relationship between diffusivity and lee-wave energy conversion (eqn 50), the impact of mixing by ocean lee waves has been examined in two ways. The first method uses the observed hydrography and the 3D map of diffusivity which results to determine the role of lee-waves in driving water mass transformations. Nikurashin & Ferrari (2013) used the energy conversion estimate from Nikurashin & Ferrari (2011), the WOCE ocean atlas density distribution to determine the stratification, local mixing fraction $q_L = 30\%$, and decay scale $\zeta = 500m$ (as used for the tidally-driven component of mixing). They conclude that lee-wave driven mixing dominates in the Southern Ocean, and accounts for about 1/3 of the global water mass transformation. Their calculation however, ignored the convergence of buoyancy flux in the bottom boundary layer. de Lavergne et al. (2016) uses the Scott et al. (2011) map for energy conversion, the WOCE hydrographic data, and again $q_L = 1/3$ and $\zeta = 500m$, to show that lee-wave driven mixing dominates south of 30°S, and with bottom boundary layer buoyancy flux convergence, leads to a lightening of the densest waters, while densifying the overlying water, with about 4 Sv of both upwelling and downwelling. Lee-wave driven mixing therefore mixes away the densest Antarctic Bottom Water in the Antarctic Circumpolar Current, while also converting some overlying Circumpolar Deep Water into AABW.

The second method to explore the impact of lee-wave driven mixing is to include a parameterization of this process directly in an ocean-climate model, and explore the response of the model stratification and circulation to the parameterized mixing. Melet et al. (2014) imposes the static energy conversion map from Nikurashin & Ferrari (2011), with $q_L = 1$ and $1/3$ and $\zeta = 300m$ and $900m$, to explore the sensitivity to these parameters. By comparison the tidally-driven mixing parameterization has $q_T = 1/3$ and $\zeta = 300m$. As in de Lavergne et al. (2016), the lee-wave driven mixing has a large impact on the diffusivity in the deep Southern Ocean, leading to a warming of the Antarctic Bottom Water, and making the Southern sinking cell of the meridional overturning circulation lighter and about

10% stronger (**Figure 5b**) , and reducing the extension of this cell into the northern hemisphere. The impact of the lee-wave driven mixing is reduced if the local fraction of dissipation is reduced from $q_L = 1$ to $q_L = 1/3$ (not accounting for the fraction of energy which does not dissipate locally), but is less sensitive to changes in the decay scale ζ. An earlier study (Saenko et al., 2012) used the eddy-energy sink map of (Zhai et al., 2010) (not directly an estimate of lee-wave energy conversion), with $q_L = 1$ and $\zeta = 300 - 1000m$, to show a similar increase in the strength of the lower overturning cell when diapycnal mixing associated with loss of energy from mesoscale eddies in included. These studies, with static energy conversion maps, cannot account for feedbacks between the mesoscale eddies and mixing. By contrast, Stanley & Saenko (2014) employs a fully temporally-varying estimate of the energy flux from the parameterized eddy field to diapycnal mixing, and explores the range of feedbacks which result in a coarse resolution ocean-climate model. However, as in the energetically-consistent sub-grid-scale model of Eden et al. (2014) the energy-conversion parameterization is based only on the mesoscale eddy energy, and includes no topographic information. A fully temporally-varying estimate of energy conversion from geostrophic flow to lee-waves has yet to be included as a component of the mixing parameterization in a realistic ocean climate model.

The idealized eddy-resolving channel model of Broadbridge et al. (2016), a representation of the Southern Ocean, does include a temporally and spatially varying parameterization of lee-wave driven mixing. The diapycnal mixing is calculated using eqn 50, with $q_L = 1$, a linear function for $F(z)$, and a time-dependent estimate of $E_L(x, y, t)$, using a (Goff & Arbic, 2010) spectral representation of topography and the instantaneous model near-bottom velocities. The sensitivity of solutions to the rms height of the topography and the magnitude of the surface wind-stress are explored. The strength of the lower overturning cell is strongly dependent on the bottom topography amplitude (consistent with (Saenko et al., 2012, Melet et al., 2014)). The mixing is sensitive to wind-stress and the lower overturning cell is therefore also sensitive to the wind-stress. This study does not apply any topographic bottom drag parameterization to the resolved flow. Trossman et al. (2013) and Trossman et al. (2016) show that the bottom drag associated with lee-waves can significantly influence the circulation, but ignore the effect of lee-waves on mixing. Future work needs to apply consistent parameterizations of lee-wave driven mixing and bottom-drag.

In summary, existing parameterizations of lee-wave driven mixing are all based on linear theory for energy conversion, perhaps with saturation at steep topography. Given that observed dissipation is much less than this linear energy conversion estimate, the mixing due to lee-waves is likely overestimated unless a small value for q_L is used. The vertical profile of this mixing in current applications is not physically based; near-bottom hydraulic jumps, as well as critical layer wave breaking and/or reabsorption are not currently represented.

5 KNOWLEDGE GAPS

We are a long way from having a full understanding of mixing by oceanic lee waves suitable for parameterizations of mixing in coarse resolution general circulation models. Particular areas of uncertainty incude:

At steep topography, how much energy is converted from the mean flow to perturbations?: While we have theoretical predictions for the energy conversion from mean flow to lee-waves for linear scenarios when $Fr_L = Nh_0/U_0 << 1$, the behavior for $Fr_L > 1$ is less clear. The flow is blocked for large Fr_L, and so the effective height of the topography over which the flow moves is reduced. The implied saturation of the energy conversion is captured by eqn 27. However, the energy input from the mean flow into the hydraulically controlled jet above the topography and the low-mode adjustment contributing to the upstream blocking are not captured by this saturation assumption. Eqn 30 attempts to capture the hydraulic effects on form drag, but ignores nonhydrostatic effects. What is the partition of energy extracted from the mean flow into vertically propagating waves versus the hydraulic flow?

How much dissipation and mixing occurs locally at the topography?: Particularly when $Fr_L > 1$, and there is blocking, what fraction of the energy converted from the mean flow is then lost to dissipation in a hydraulic jump? By contrast, how much energy is lost from the hydraulic flow to internal waves radiating upward from the hydraulic jump? How do the external parameters (e.g. topography, stratification, flow speed) influence the energy lost in the hydraulic jump? What role do boundary-layer frictional processes play in determining the relative importance of local dissipation?

Where do propagating lee waves break or otherwise lose their energy?: Possible candidates, in addition to near the topography, include: energy transfer to near-inertial waves which dissipate locally due to their high vertical wavenumbers (Nikurashin & Ferrari, 2010b); critical layer processes associated with changes in stratification and background flow (Kunze & Lien, 2019); breaking downstream of the topography (Zheng & Nikurashin, 2019). No parameterization as yet attempts to account for these physical mechanisms of lee-wave breaking or reabsorption,

modulated by mesoscale and larger variations in stratification and circulation, and the way in which they influence the spatial distribution of the lee-wave induced diffusivity relative to the distribution of the energy source for the waves.

What feedbacks occur between the stratification, mesoscale eddies and lee-wave driven mixing in a realistic climate model?: While some large-scale circulation models have connected the mesoscale eddy energy loss to mixing, and examined the impact on the large-scale flow (Stanley & Saenko, 2014), these models have not incorporated lee-wave theory to tie this energy transfer to topography. Lee-wave parameterizations have only been implemented in static form in global circulation models (Melet et al., 2014), or in a fully time-evolving form in an idealized model (Broadbridge et al., 2016), and the associated bottom drag has not been included. We have not yet fully explored the influence of lee wave–driven mixing in a realistic global model where the energy conversion varies spatially and temporally as a function of changing mesoscale eddy velocities and stratification. Such a model will allow lee wave–driven changes in mixing to influence the stratification, in turn influencing the mesoscale eddy field and creating a feedback loop with lee wave generation.

[SUMMARY POINTS]

1. Ocean lee-waves are generated by both geostrophic and oscillating tidal flow over sea-floor topography.
2. Ocean lee-waves are a mechanism for transferring mechanical energy from the larger scales of geostrophic motion or barotropic tides to smaller vertical scales where turbulent mixing can occur.
3. For small amplitude topography, the rate at which energy is converted from geostrophic flow to lee-waves is well understood.
4. For larger amplitude topography, blocking of the flow occurs, the energy conversion rate to propagating waves may saturate, and some energy is converted to a hydraulically controlled jet and dissipated in a hydraulic jump.
5. The eventual fate of propagating lee-wave energy may include wave breaking, mixing, and dissipation in critical layers, or reabsorption by the large-scale flow.
6. Parameterizations of mixing by ocean lee-waves employ linear theory of energy conversion, modified to include saturation, but do not include the localization of energy dissipation and mixing in hydraulic jumps and critical layers, or the reabsorption of wave energy by the large-scale flow.

DISCLOSURE STATEMENT

The author is not aware of any affiliations, memberships, funding, or financial holdings that might be perceived as affecting the objectivity of this review.

ACKNOWLEDGMENTS

This review was prepared by Sonya Legg under award NA18OAR4320123 from the National Oceanic and Atmospheric Administration, U.S. Department of Commerce. The statements, findings, conclusions, and recommendations are those of the author and do not necessarily reflect the views of the National Oceanic and Atmospheric Administration, or the U.S. Department of Commerce. The author thanks Jody Klymak, Stephanie Waterman, Ruth Musgrave, Eric Mayer, Maxim Nikurashin, Angelique Melet, and Bruce Sutherland for conversations, comments, and suggestions which helped in the development of this review.

References

Adcroft A, Hallberg R, Dunne JP, Samuels BL, Galt JA, et al. 2010. Simulations of underwater plumes of dissolved oil in the gulf of mexico. *Geophysical Research Letters* 37

Aguilar DA, Sutherland BR. 2006. Internal wave generation from rough topography. *Physics of Fluids* 18:066603

Alexander MJ, Teitelbaum H. 2011. Three-dimensional properties of andes mountain waves observed by satellite: A case study. *Journal of Geophysical Research: Atmospheres* 116

Alford MH, Klymak JM, Carter GS. 2014. Breaking internal lee waves at kaena ridge, hawaii. *Geophysical Research Letters* 41:906–912

Alford MH, Peacock T, MacKinnon JA, Nash JD, Buijsman MC, et al. 2015. The formation and fate of internal waves in the south china sea. *Nature* 521:65–69

Bell TH. 1975. Lee waves in stratified flows with simple harmonic time dependence. *Journal of Fluid Mechanics* 67:705–722

Bell Jr. TH. 1975. Topographically generated internal waves in the open ocean. *Journal of Geophysical Research (1896-1977)* 80:320–327

Booker JR, Bretherton FP. 1967. The critical layer for internal gravity waves in a shear flow. *Journal of Fluid Mechanics* 27:513–539

Brearley JA, Sheen KL, Naveira Garabato AC, Smeed DA, Waterman S. 2013. Eddy-induced modulation of turbulent dissipation over rough topography in the southern ocean. *Journal of Physical Oceanography* 43:2288–2308

Broad AS. 1995. Linear theory of momentum fluxes in 3-d flows with turning of the mean wind with height. *Quarterly Journal of the Royal Meteorological Society* 121:1891–1902

Broadbridge MB, Naveira Garabato AC, Nurser AJG. 2016. Forcing of the overturning circulation across a circumpolar channel by internal wave breaking. *Journal of Geophysical Research: Oceans* 121:5436–5451

Clément L, Frajka-Williams E, Sheen KL, Brearley JA, Garabato ACN. 2016. Generation of internal waves by eddies impinging on the western boundary of the north atlantic. *Journal of Physical Oceanography* 46:1067–1079

Clément L, Thurnherr AM, St. Laurent LC. 2017. Turbulent mixing in a deep fracture zone on the mid-atlantic ridge. *Journal of Physical Oceanography* 47:1873–1896

Conover JH. 1964. The identification and significance of orographically induced clouds observed by tiros satellites. *Journal of Applied Meteorology* 3:226–234

Cusack JM, Naveira Garabato AC, Smeed DA, Girton JB. 2017. Observation of a large lee wave in the drake passage. *Journal of Physical Oceanography* 47:793–810

da Silva J, New A, Magalhaes J. 2011. On the structure and propagation of internal solitary waves generated at the mascarene plateau in the indian ocean. *Deep Sea Research Part I: Oceanographic Research Papers* 58:229 – 240

Dale AC, Inall ME. 2015. Tidal mixing processes amid small-scale, deep-ocean topography. *Geophysical Research Letters* 42:484–491

de Lavergne C, Madec G, Le Sommer J, Nurser AJG, Naveira Garabato AC. 2016. On the consumption of antarctic bottom water in the abyssal ocean. *Journal of Physical Oceanography* 46:635–661

de Marez C, Lahaye N, Gula J. 2020. Interaction of the gulf stream with small scale topography: a focus on lee waves. *Scientific Reports* 10

Dossmann Y, G. Rosevear M, Griffiths RW, McC. Hogg A, Hughes GO, Copeland M. 2016. Experiments with mixing in stratified flow over a topographic ridge. *Journal of Geophysical Research: Oceans* 121:6961–6977

Drazin PG. 1961. On the steady flow of a fluid of variable density past an obstacle. *Tellus* 13:239–251

Eden C, Czeschel L, Olbers D. 2014. Toward energetically consistent ocean models. *Journal of Physical Oceanography* 44:3160–3184

Eden C, Greatbatch RJ. 2008. Diapycnal mixing by meso-scale eddies. *Ocean Modelling* 23:113 – 120

Farmer D, Armi L. 1999. Stratified flow over topography: the role of small-scale entrainment and mixing in flow establishment. *Proceedings of the Royal Society of London. Series A: Mathematical, Physical and Engineering Sciences* 455:3221–3258

Ferrari R, Wunsch C. 2009. Ocean circulation kinetic energy: Reservoirs, sources, and sinks. *Annual Review of Fluid Mechanics* 41:253–282

Garrett C, Kunze E. 2007. Internal tide generation in the deep ocean. *Annual Review of Fluid Mechanics* 39:57–87

Goff JA. 2010. Global prediction of abyssal hill root-mean-square heights from small-scale altimetric gravity variability. *Journal of Geophysical Research: Solid Earth* 115

Goff JA, Arbic BK. 2010. Global prediction of abyssal hill roughness statistics for use in ocean models from digital maps of paleo-spreading rate, paleo-ridge orientation, and sediment thickness. *Ocean Modelling* 32:36 – 43. The magic of modelling: A special volume commemorating the contributions of Peter D. Killworth - Part I

Goff JA, Jordan TH. 1988. Stochastic modeling of seafloor morphology: Inversion of sea beam data for second-order statistics. *Journal of Geophysical Research: Solid Earth* 93:13589–13608

Gonella J. 1972. A rotary-component method for analysing meteorological and oceanographic vector time series. *Deep Sea Research and Oceanographic Abstracts* 19:833–846

Gouretski V, Koltermann K. 2004. Woce global hydrograhic climatology. *erichte des BSH 35. 52. ISSN: 0946-6010*

Gregg M. 1989. Scaling turbulent dissipation in the thermocline. *J. Geophys. Res.* 94:9686–9698

Gregg M, Sanford T, Winkel D. 2003. Reduced mixing from the breaking of internal waves in equatorial waters. *Nature* 422:513–5

Henyey FS, Wright J, Flatté SM. 1986. Energy and action flow through the internal wave field: An eikonal approach. *Journal of Geophysical Research: Oceans* 91:8487–8495

Klymak JM. 2018. Nonpropagating form drag and turbulence due to stratified flow over large-scale abyssal hill topography. *Journal of Physical Oceanography* 48:2383–2395

Klymak JM, Gregg MC. 2003. The role of upstream waves and a downstream density pool in the growth of lee waves: Stratified flow over the knight inlet sill. *Journal of Physical Oceanography* 33:1446–1461

Klymak JM, Legg S, Pinkel R. 2010a. High-mode stationary waves in stratified flow over large obstacles. *Journal of Fluid Mechanics* 644:321–336

Klymak JM, Legg S, Pinkel R. 2010b. A simple parameterization of turbulent tidal mixing near supercritical topography. *Journal of Physical Oceanography* 40:2059–2074

Klymak JM, Legg SM. 2010. A simple mixing scheme for models that resolve breaking internal waves. *Ocean Modelling* 33:224 – 234

Klymak JM, Pinkel R, Rainville L. 2008. Direct breaking of the internal tide near topography: Kaena ridge, hawaii. *Journal of Physical Oceanography* 38:380–399

Konyaev K, Sabinin K, Serebryany A. 1995. Large-amplitude internal waves at the mascarene ridge in the indian ocean. *Deep Sea Research Part I: Oceanographic Research Papers* 42:2075 – 2091

Kunze E, Lien RC. 2019. Energy sinks for lee waves in shear flow. *Journal of Physical Oceanography* 49:2851–2865

Köhler J, Mertens C, Walter M, Stöber U, Rhein M, Kanzow T. 2014. Variability in the internal wave field induced by the atlantic deep western boundary current at 16°n. *Journal of Physical Oceanography* 44:492–516

Legg S, Klymak J. 2008. Internal hydraulic jumps and overturning generated by tidal flow over a tall steep ridge. *Journal of Physical Oceanography* 38:1949–1964

Liang X, Thurnherr AM. 2012. Eddy-modulated internal waves and mixing on a midocean ridge. *Journal of Physical Oceanography* 42:1242–1248

Long RR. 1955. Some aspects of the flow of stratified fluids. *Tellus* 7:341–357

MacKinnon JA, Zhao Z, Whalen CB, Waterhouse AF, Trossman DS, et al. 2017. Climate process team on internal wave–driven ocean mixing. *Bulletin of the American Meteorological Society* 98:2429–2454

Marshall DP, Adcroft AJ. 2010. Parameterization of ocean eddies: Potential vorticity mixing, energetics and arnold's first stability theorem. *Ocean Modelling* 32:188 – 204. The magic of modelling: A special volume commemorating the contributions of Peter D. Killworth – Part 2

Mayer FT, Fringer OB. 2017. An unambiguous definition of the froude number for lee waves in the deep ocean. *Journal of Fluid Mechanics* 831:R3

McFarlane NA. 1987. The effect of orographically excited gravity wave drag on the general circulation of the lower stratosphere and troposphere. *Journal of the Atmospheric Sciences* 44:1775–1800

Melet A, Hallberg R, Adcroft A, Nikurashin M, Legg S. 2015. Energy flux into internal lee waves: Sensitivity to future climate changes using linear theory and a climate model. *Journal of Climate* 28:2365–2384

Melet A, Hallberg R, Legg S, Nikurashin M. 2014. Sensitivity of the ocean state to lee wave-driven mixing. *Journal of Physical Oceanography* 44:900–921

Meyer A, Polzin KL, Sloyan BM, Phillips HE. 2016. Internal waves and mixing near the kerguelen plateau. *Journal of Physical Oceanography* 46:417–437

Meyer A, Sloyan BM, Polzin KL, Phillips HE, Bindoff NL. 2015. Mixing variability in the southern ocean. *Journal of Physical Oceanography* 45:966–987

Musgrave RC, MacKinnon JA, Pinkel R, Waterhouse AF, Nash J. 2016a. Tidally driven processes leading to near-field turbulence in a channel at the crest of the mendocino escarpment. *Journal of Physical Oceanography* 46:1137–1155

Musgrave RC, MacKinnon JA, Pinkel R, Waterhouse AF, Nash J, Kelly SM. 2017. The influence of subinertial internal tides on near-topographic turbulence at the mendocino ridge: Observations and modeling. *Journal of Physical Oceanography* 47:2139–2154

Musgrave RC, Pinkel R, MacKinnon JA, Mazloff MR, Young WR. 2016b. Stratified tidal flow over a tall ridge above and below the turning latitude. *Journal of Fluid Mechanics* 793:933–957

Nakamura T, Awaji T, Hatayama T, Akitomo K, Takizawa T, et al. 2000. The generation of large-amplitude unsteady lee waves by subinertial k1 tidal flow: A possible vertical mixing mechanism in the kuril straits. *Journal of Physical Oceanography* 30:1601–1621

Nikurashin M, Ferrari R. 2010a. Radiation and dissipation of internal waves generated by geostrophic motions impinging on small-scale topography: Application to the southern ocean. *Journal of Physical Oceanography* 40:2025–2042

Nikurashin M, Ferrari R. 2010b. Radiation and dissipation of internal waves generated by geostrophic motions impinging on small-scale topography: Theory. *Journal of Physical Oceanography* 40:1055–1074

Nikurashin M, Ferrari R. 2011. Global energy conversion rate from geostrophic flows into internal lee waves in the deep ocean. *Geophysical Research Letters* 38

Nikurashin M, Ferrari R. 2013. Overturning circulation driven by breaking internal waves in the deep ocean. *Geophysical Research Letters* 40:3133–3137

Nikurashin M, Ferrari R, Grisouard N, Polzin K. 2014. The impact of finite-amplitude bottom topography on internal wave generation in the southern ocean. *Journal of Physical Oceanography* 44:2938–2950

Osborn TR. 1980. Estimates of the local rate of vertical diffusion from dissipation measurements. *Journal of Physical Oceanography* 10:83–89

Palmer TN, Shutts GJ, Swinbank R. 1986. Alleviation of a systematic westerly bias in general circulation and numerical weather prediction models through an orographic gravity wave drag parametrization. *Quarterly Journal of the Royal Meteorological Society* 112:1001–1039

Peltier WR, Clark TL. 1979. The evolution and stability of finite-amplitude mountain waves. part ii: Surface wave drag and severe downslope windstorms. *Journal of the Atmospheric Sciences* 36:1498–1529

Rippeth TP, Lincoln BJ, Lenn YD, Green JAM, Sundfjord A, Bacon S. 2015. Tide-mediated warming of arctic halocline by atlantic heat fluxes over rough topography. *Nature Geoscience* 8:191–194

Rippeth TP, Vlasenko V, Stashchuk N, Scannell BD, Green JAM, et al. 2017. Tidal conversion and mixing poleward of the critical latitude (an arctic case study). *Geophysical Research Letters* 44:12,349–12,357

Saenko OA, Zhai X, Merryfield WJ, Lee WG. 2012. The combined effect of tidally and eddy-driven diapycnal mixing on the large-scale ocean circulation. *Journal of Physical Oceanography* 42:526–538

Scorer RS. 1949. Theory of waves in the lee of mountains. *Quarterly Journal of the Royal Meteorological Society* 75:41–56

Scott RB, Goff JA, Naveira Garabato AC, Nurser AJG. 2011. Global rate and spectral characteristics of internal gravity wave generation by geostrophic flow over topography. *Journal of Geophysical Research: Oceans* 116

Shakespeare CJ, Hogg AM. 2017. The viscous lee wave problem and its implications for ocean modelling. *Ocean Modelling* 113:22 – 29

Sheen KL, Brearley JA, Naveira Garabato AC, Smeed DA, Laurent LS, et al. 2015. Modification of turbulent dissipation rates by a deep southern ocean eddy. *Geophysical Research Letters* 42:3450–3457

Sheen KL, Brearley JA, Naveira Garabato AC, Smeed DA, Waterman S, et al. 2013. Rates and mechanisms of turbulent dissipation and mixing in the southern ocean: Results from the diapycnal and isopycnal mixing experiment in the southern ocean (dimes). *Journal of Geophysical Research: Oceans* 118:2774–2792

Sloyan BM. 2005. Spatial variability of mixing in the southern ocean. *Geophysical Research Letters* 32

SMITH RB. 1989. Mountain-induced stagnation points in hydrostatic flow. *Tellus A* 41A:270–274

St. Laurent L, Naveira Garabato AC, Ledwell JR, Thurnherr AM, Toole JM, Watson AJ. 2012. Turbulence and diapycnal mixing in drake passage. *Journal of Physical Oceanography* 42:2143–2152

St. Laurent LC, Simmons HL, Jayne SR. 2002. Estimating tidally driven mixing in the deep ocean. *Geophysical Research Letters* 29:21–1–21–4

Stanley GJ, Saenko OA. 2014. Bottom-enhanced diapycnal mixing driven by mesoscale eddies: Sensitivity to wind energy supply. *Journal of Physical Oceanography* 44:68–85

Teixeira MAC. 2014. The physics of orographic gravity wave drag. *Frontiers in Physics* 2:43

Thurnherr AM, St. Laurent LC. 2011. Turbulence and diapycnal mixing over the east pacific rise crest near 10°n. *Geophysical Research Letters* 38

Thurnherr AM, St. Laurent LC, Speer KG, Toole JM, Ledwell JR. 2005. Mixing associated with sills in a canyon on the midocean ridge flank. *Journal of Physical Oceanography* 35:1370–1381

Trossman DS, Arbic BK, Garner ST, Goff JA, Jayne SR, et al. 2013. Impact of parameterized lee wave drag on the energy budget of an eddying global ocean model. *Ocean Modelling* 72:119 – 142

Trossman DS, Arbic BK, Richman JG, Garner ST, Jayne SR, Wallcraft AJ. 2016. Impact of topographic internal lee wave drag on an eddying global ocean model. *Ocean Modelling* 97:109 – 128

Waterman S, Naveira Garabato AC, Polzin KL. 2013. Internal waves and turbulence in the antarctic circumpolar current. *Journal of Physical Oceanography* 43:259–282

Waterman S, Polzin KL, Naveira Garabato AC, Sheen KL, Forryan A. 2014. Suppression of internal wave breaking in the antarctic circumpolar current near topography. *Journal of Physical Oceanography* 44:1466–1492

Watson AJ, Ledwell JR, Messias MJ, King BA, Mackay N, et al. 2013. Rapid cross-density ocean mixing at mid-depths in the drake passage measured by tracer release. *Nature* 501:408–411

Welch WT, Smolarkiewicz P, Rotunno R, Boville BA. 2001. The large-scale effects of flow over periodic mesoscale topography. *Journal of the Atmospheric Sciences* 58:1477–1492

Wijesekera H, Padman L, Dillon T, Levine M, Paulson C, Pinkel R. 1993. The application of internal-wave dissipation models to a region of strong mixing. *Journal of Physical Oceanography* 23:269–286

Winters KB. 2016. The turbulent transition of a supercritical downslope flow: sensitivity to downstream conditions. *Journal of Fluid Mechanics* 792:997–1012

Winters KB, Armi L. 2012. Hydraulic control of continuously stratified flow over an obstacle. *Journal of Fluid Mechanics* 700:502–513

Winters KB, Armi L. 2013. The response of a continuously stratified fluid to an oscillating flow past an obstacle. *Journal of Fluid Mechanics* 727:83–118

Winters KB, Armi L. 2014. Topographic control of stratified flows: upstream jets, blocking and isolating layers. *Journal of Fluid Mechanics* 753:80–103

Winters KB, Lombard PN, Riley JJ, D'Asaro EA. 1995. Available potential energy and mixing in density-stratified fluids. *Journal of Fluid Mechanics* 289:115–128

Winters KB, Riley JJ. 1992. Instability of internal waves near a critical level. *Dynamics of Atmospheres and Oceans* 16:249 – 278

Wright CJ, Scott RB, Ailliot P, Furnival D. 2014. Lee wave generation rates in the deep ocean. *Geophysical Research Letters* 41:2434–2440

Wurtele MG, Sharman RD, Datta A. 1996. Atmospheric lee waves. *Annual Review of Fluid Mechanics* 28:429–476

Yang L, Nikurashin M, Hogg AM, Sloyan BM. 2018. Energy loss from transient eddies due to lee wave generation in the southern ocean. *Journal of Physical Oceanography* 48:2867–2885

Zhai X, Johnson HL, Marshall DP. 2010. Significant sink of ocean-eddy energy near western boundaries. *Nature Geoscience* 3:608–612

Zheng K, Nikurashin M. 2019. Downstream propagation and remote dissipation of internal waves in the southern ocean. *Journal of Physical Oceanography* 49:1873–1887